International Journal of Fatigue 162 (2022) 107006

Contents lists available at ScienceDirect

International Journal of Fatigue

journal homepage: www.elsevier.com/locate/ijfatigue

Fatigue improvement and residual stress relaxation of shot-peened alloy steel DIN 34CrNiMo6 under axial loading

Nelson Leguinagoicoa [a], Joseba Albizuri [a,*], Aitor Larrañaga [b]

[a] Department of Mechanical Engineering, Faculty of Engineering, University of the Basque Country UPV/EHU, Bilbao, Bizkaia, Spain
[b] SGiker, University of the Basque Country UPV/EHU, Leioa, Bizkaia, Spain

ARTICLE INFO

Keywords:
34CrNiMo6 steel
High-cycle fatigue
Shot-peening
Residual stresses
Relaxation of residual stresses
Cyclic relaxation

ABSTRACT

Shot-peening treatment was applied to a quenched and tempered DIN 34CrNiMo6 steel to improve its high-cycle R: −1 axial fatigue strength. Compared with the machined condition, the increase in the fatigue limit was 21.8%. S-N curves for shot-peened and the as machined condition were presented and compared with those obtained in previous research for rotating bending fatigue, including curves for mirror-polished specimens.

The applied shot-peening treatment in this work (I_{sp}: 8A and 200% coverage) for quenched and tempered (Q + T) DIN 34CrNiMo6 steel introduced a compressive residual stress field and an increase in surface roughness, as well as minor variations in microstructure, hardness and the FWHM (full width of the diffraction peak at half maximum intensity) parameter.

The introduced compressive residual stress field tended to reduce when an external stress is applied. This was due to the onset of plastic strain. In this paper, two types of quasi-static tests were conducted by applying an axial stress with six different magnitudes and in the two directions (compressive or tensile). This was in order to assess their influence on the relaxation of surface residual stresses. Due to the introduced compressive residual stresses, if the applied stress was compressive, the onset of plastic deformations was achieved with a lower stress magnitude.

In addition, surface residual stress relaxation under cyclic applied stress was evaluated at four different stress magnitudes. Due to the cyclic-softening behaviour of this Q + T steel, its cyclic mechanical properties must be considered to assess the onset of plastic strains. With the experimental data, a logarithmic model to predict the evolution of surface residual stresses with the number of cycles for different applied stress magnitudes was presented.

1. Introduction

A common practise in mechanical engineering for the manufacture of high-performance metallic components is by the application of mechanical treatment, typically performed as the last step in the manufacturing process with the aim of improving their resistance to fatigue, wear [1] or corrosion [2].

Shot-peening [3] is one of the most widely forms of mechanical treatment and is the scope of this work. This treatment consists of continuously bombarding the surface of the mechanical parts with small and hard shots at high speed. By this way, plastic deformations are generated on the surface of the mechanical component that is treated. These plastic (macro)deformations on the surface layers generate an equi-biaxial compressive residual stress field [4]. The introduction of compressive residual stresses, on the surface and at the inner layers very close to the surface [5], erases the remaining tensile residual stresses from the manufacturing process [6], which favor premature fatigue failure by facilitating crack nucleation and growth [7]. In contrast, compressive residual stresses that are introduced on the surface zone, delay or block crack growth [8]. Usually, an improvement in fatigue behavior is obtained in treated parts with respect to untreated parts [9]. This is true even while taking into account that shot-peening produces a worsening of surface roughness [10]. Moreover, the shot-peening treatment, due to the cold-working on the treated part, produces a variation of its microhardness, the number of dislocations and the level of distortion of the crystallography. These variations are usually quantified within the (full width of the diffraction peak at half maximum intensity) FWHM parameter, which evaluates the variation of the micro-

* Corresponding author.
E-mail address: joseba.albizuri@ehu.eus (J. Albizuri).

https://doi.org/10.1016/j.ijfatigue.2022.107006
Received 3 March 2022; Received in revised form 26 April 2022; Accepted 9 May 2022
Available online 13 May 2022

deformations [11].

The main effect of shot-peening is the generation of a compressive residual stress field on the surface and subsurface area. The profile (magnitude, depth and gradient) of this stress field depends on the intensity of the shot-peening process [12], the coverage (exposure time) used during the treatment [13] and the material type and properties of the treated part. These residual stresses generated by mechanical treatment tend to reduce thermally or mechanically, either under quasi-static loading or variable load cycles [14]. This reduction of residual stresses is commonly referred to as stress relaxation.

The relaxation of residual stresses depends on the nature of the residual stresses, the material properties and its microstructure [15]. The main mechanism of stress relaxation due to external mechanical loading is based on the generation of plastic strains in the material as a consequence of the movement of dislocations [16]. Because of this relaxation, it is not possible to include the initial residual stresses directly as a mean stress in the fatigue life calculation [17].

The generation of residual stresses by shot-peening and their relaxation under cyclic loading is widely studied in steel alloys. It is known that the residual stress field generated varies according to the type of steel, whether it is in normalized condition [18] or in Q + T condition [19]. Also, the tempering temperature [20] varies the generated residual stress field. It is noticed that, with softer steels, shot-peening produces higher work-hardening [21]. On the other hand, with harder steels, cold-work tends to generate work-softening, which favors stress relaxation under cyclic loading. For a normalized steel under strain-controlled fatigue cycles, a direct relationship between stress relaxation and the variation of the FWHM parameter is observed [22]. Residual stress relaxation under cyclic loading directly affects the improvement of fatigue strength [23]. Similar studies are found for other metal alloys, such as; stainless steel [24], the aluminum alloys 6082-T5 [25] and 7075-T651 [26], titanium alloy Ti-6Al-4V [27] and in Nickel-base alloy IN100 [28].

To further optimize fatigue improvement, other alternative mechanical treatments or variations of traditional shot-peening have been developed. By their different nature, they change the surface roughness of the treated part or generate different residual stress field profiles (deeper or with greater magnitude) and reduce the level of cold-work on the material microstructure, with the aim of reducing or delaying the residual stresses relaxation [29]. Examples of these mechanical treatments are dual shot-peening (DSP), warm shot-peening (WSP) [30 31], shot-peening plus short-annealing [32], severe shot-peening (SSP) [33 34], laser shock-peening (LSP) [35] or low-plasticity burnishing (LPB) [36].

Most of these treatments are presented in comparison with shot-peening for the same material. For example, in [37] a 4140 steel is treated by LSP and SP and then, the mechanical properties and effects generated by each mechanical treatment are compared. In [29] SP, LSP and LPB are compared for a Nickel-base alloy IN718. In addition, a model for predicting the residual stress relaxation at the surface is proposed. As a result, this model has been adapted for a 304 stainless steel in [38]. Kodama proposed one of the first relaxation models [39], whose reduction with the number of load cycles is logarithmic. Within previous investigations within our department, other prediction models based on logarithmic factor, have been proposed [40] & [41].

This paper presents a direct continuation of previous research developed by the Mechanical Engineering Department of ETSIB (EHU-UPV), where rotating bending fatigue performance of Q + T steel DIN 34CrNiMo6 and the effect of mechanical treatments, such as, low-plasticity burnishing (LPB) and shot-peening (SP) were studied [41]. The axial fatigue limit of this material considering the effect of mean stresses was already analysed [42]. Before those studies, the influence of LPB on surface properties [43] and HC fatigue with steel AISI 1045 was evaluated [40].

In the present work, the effect of a shot-peening treatment on the surface properties, microstructure and residual stresses in a quenched and tempered steel was analyzed. The improvement in axial fatigue strength produced by shot-peening was studied in direct comparison with an as-machined condition. Simple quasi-static tests were proposed to better understand the mechanisms of residual stress relaxation. These tests served as a reference for the study of residual stress relaxation on the specimen surface during the fatigue process. In addition, a general model for predicting the evolution of residual stresses on the surface as a function of the applied stress and the number of cycles was proposed. Finally, the appearance and evolution of cracks on the ruptured sections of the studied cases under cyclic loading was shown.

2. Base material properties and specimen description

2.1. Base material description

Testing specimens were manufactured from 30 mm diameter steel rolled bars, supplied by *Thyssen-Krupp Materials Ibérica, S.A*. This steel is defined according to DIN 34CrNiMo6, which is a high-resistance steel, widely employed in mechanical components that require an important level of exigency. A certificate of the chemical composition was also provided by the supplier, which is presented in Table 1. The base material is served as quenched and tempered condition. The austenitizing temperature for oil-quenching is 900º C and tempering is conducted at 570º C. The tempering temperature directly affects the grain size and hardness for these types of steels [20].

Tensile quasi-static tests were developed, following the UNE-EN ISO 6892-1 standard [44] with specimens prepared according to DIN 50113. This was in order to obtain static mechanical properties of this ductile steel. Results for the tests are summarized in Table 2. Values obtained are in accordance with those that can be found in the literature for this same steel [6,45] & [46].

This steel in Q + T condition, tends to develop cyclic-softening when a cyclic load is applied [47]. This means that the cyclic yield point is lower than the monotonic yield point. The empirical relation between $\sigma_{yp}/\sigma_{yp} = 1.12 < 1.2$ as proposed in [48] is fulfilled, which identifies this property. Monotonic strength values obtained for the base material are slightly higher (+~10%) than those observed in data within literature. For this reason, the estimated cyclic yield point is set at 825 MPa.

2.2. Specimens: As machined and shot-peened

A batch of hourglass testing samples were manufactured in accordance with specifications for axial fatigue test following the ASTM E466-15 [49]. The main dimensions of the hourglass test specimens can be observed in Fig. 1.

Machined specimens used for testing remain without a polished finish. Some of them, were subjected to a shot-peening process on their whole surface. So, in this paper, in order to study the effect of shot-peening process, two kinds of specimens are presented; machined and shot-peened (SP). The shot-peening process parameters used are the same as those applied in previous research [41] and they can be seen in Table 3.

2.3. Hardness & microstructure

Hardness was measured on the surface, before cutting the samples. Then, the microhardness, according to ISO 4545-1:2018 was measured up to 0.5 mm depth, for the two kinds of specimens. The results are summarized in Table 4 and presented graphically in Fig. 2. It can be observed that the shot-peening treatment produces a weak increase in the hardness at approximately of 1.68 HRC (4.4%) on the surface and near-surface area, up to a depth close to 0.2 mm. Shot-peening applied to this steel does not generate a noticeable increase in hardness, in which its slight increase is likely related to the presence of the residual stress field.

For the base material, the applied thermal treatment generates a

Table 1
Chemical composition of 34CrNiMo6 Q + T steel, (at.%).

C	Cr	Ni	Mn	Si	Mo	P	S	Fe
0.340	1.560	1.500	0.700	0.270	0.237	0.007	0.003	balance

Table 2
Monotonic mechanical properties of 34CrNiMo6 samples.

Yield strength σ_{yp}	Ultimate tensile strength σ_{ut}	Ultimate tensile strain ε_{ut}	Area reduction Z
1.084 MPa	1.209 MPa	12.18%	60.17%

hard steel with fine and uniform microstructure with fine-tempered martensite giving G8 (ASTM) grain size. This can be seen in Fig. 3. The shot-peening treatment produces irregularities on the surface. However, there are no significant modifications on the areas near to the surface. Only could be appreciated a slight sub-superficial deformation layer of approximately 20–25 μm in the SP specimen.

2.4. Surface roughness and topography

For the two different kinds of specimens, the 2D profile and the 3D topography were measured with an optical profilometer on an area of 0,95x2,4 mm^2, located on the central plane of symmetry of the specimen. Measurements were according to ISO 4287 and ASME B46.1 standard, using a Gaussian filter with a 0.8 mm cut-off.

In Fig. 4 ***(a)*** a detailed view of the machined sample is shown, where the usual shape of the tooling marks can be appreciated. In Fig. 4 ***(b)*** the SP surface shows a marbled shape, with deep peaks and valleys, characteristic of shot-peening, which produces severe plastic deformation on the surface. With a coverage of 200%, the SP surface displays the impact marks as widely overlapped.

The roughness profile was evaluated on the mid plane of the sample, along the longitudinal axis, for both specimens. Roughness values are summarized in Table 5. The machined specimens show an average Ra of 0.81 μm and the SP samples display, as expected, higher roughness value than the machined specimens. For the SP samples the Ra rises up to 1.93 μm. Table 5 is also presents the roughness of mirror polished samples, as obtained in previous research [42].

2.5. Residual stresses

For all of the SP specimens studied in this work, the initial compressive residual stresses introduced by shot-peening treatment were measured on a point of the surface on their mid-plane (Fig. 1) by using the X-ray diffraction (XRD) technique [50] and following the UNE-EN 15305 standard. Measurements were developed in the X-ray diffraction Lab. of SGIker (Leioa, Spain).

The residual stress of each sample was tested using a Bruker D8 Discover diffractometer equipped with a Cr Twist tube, V filter (λ = 2.2911 Å), PolyCapTM (1 m single crystal cylinders) system for parallel beam generation (divergence of 0.25°), and a 1-D LynxEye detector (active length in 2θ 2.7°). The samples were mounted on an Eulerian Cradle with an automatically controlled X-Y-Z stage. Data were collected from range 151° to 160° 2θ (step size = 0.05 and time per step = 1 s). Strain values in the side inclination mode were recorded for different sample tilt angles (Psi) of eight steps, 0–0.7 range in Sin2ψ (0°, 18.4°, 26.6°, 33.2°, 39.2°, 45.0°, 50.8° and 56.8°) at constant azimuth angles (phi). Strain vs. Sin2ψ was plotted to estimate the stress values. In order to acquire a complete evaluation, at least 6 measurements are needed on Strain-Sin2ψ plot using three different values of (phi), 0°, 45°, 90° chosen in negative and positive values. The stress has been evaluated from strain values using the Young's modulus (E: 220,264 MPa), the Poisson ratio (ν: 0.280) and taking into consideration the elastic constants at s_1 (-1.271×10^{-6}) and at ½ s_2 (5.811×10^{-6}) of the material. A single ferrite (bcc) peak (2 1 1), available at 156° of 2θ, was used for

Table 3
Shot-Peening process parameters.

SP	
Intensity	0.008A (8A)
Flow	3 kg/min
Speed	250 mm/min
Distance	200 mm
Rotation speed	30 r.p.m.
Shot size	S230 (~0.7 mm)
Shot shape	Quasi-spherical
Shot hardness	58–60 HRC
Coverage	200%

Table 4
Machined & Shot-peened (SP) specimens' hardness in depth measurements.

Depth [mm]	Machined **Hardness [HRC]**	SP **Hardness [HRC]**
0.00	37.9	39.8
0.10	38.8	39.7
0.15	37.9	39.9
0.20	38.8	38.1
0.25	38.0	38.2
0.30	37.7	37.8
0.35	38.5	37.5
0.40	38.3	38.2
0.45	38.0	37.4
0.50	37.6	38.1

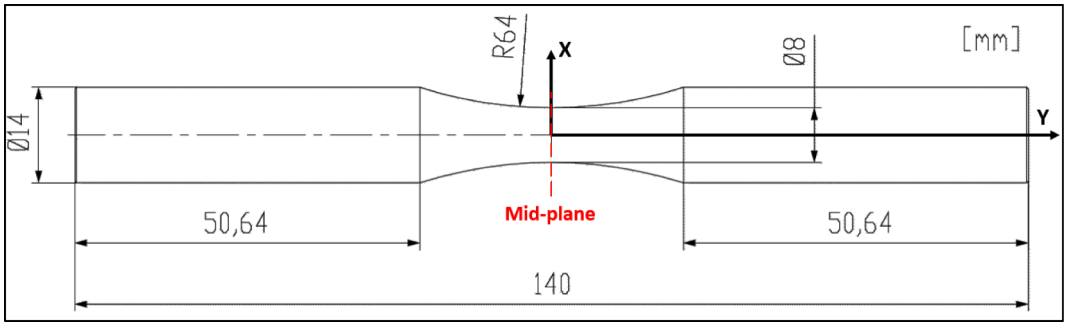

Fig. 1. General dimensions of hourglass specimens.

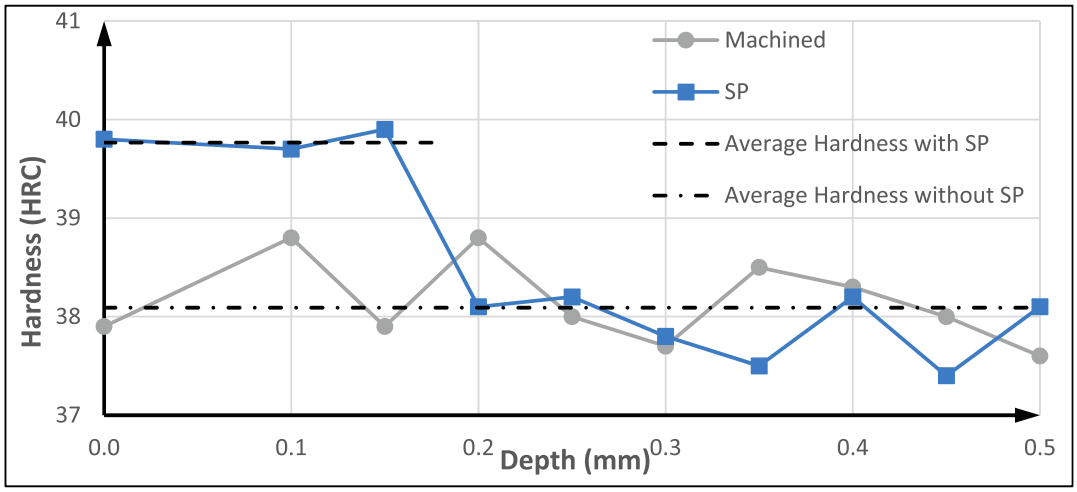

Fig. 2. In depth hardness measurements.

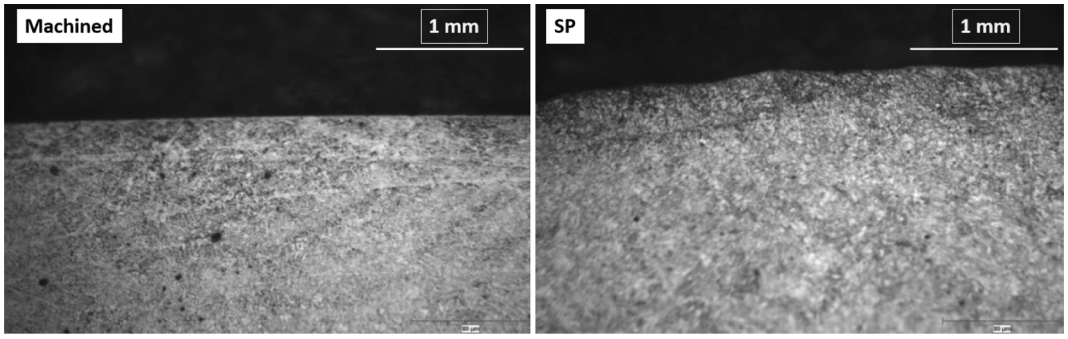

Fig. 3. Microstructure of specimens: **(a)** Machined and **(b)** shot-peened (SP).

the analysis. The obtained results were adjusted using Leptos 7.03 software from Bruker AXS GmbH. The data were corrected for absorption, background (five points at edges), polarization, smooth and K-alpha2 subtraction, the peak evaluation was fitted by the Pearson VII function. The determined values were obtained using a biaxial mode with Psi splitting function due to the shear stress components.

With this technique, the complete surface residual stress tensor is provided. The average value measured for each stress tensor component is presented in the Table 6. It can be noticed that the main values with greater magnitude, correspond to the longitudinal and the transversal components. In this case, there is a difference of 25% in the magnitude of both components. This is most certainly caused by the non-cylindrical (R: 64 mm) shape of the specimens [11]. The average surface residual stress magnitude, expressed by terms of the von Misses equivalent stress is −642.9 MPa. As seen in Fig. 5, where the mid cross-section of the specimen is shown, it can be easily explained that the direction of these components and measurement point is according to the geometry of the samples.

Measurements of initial residual stresses were extended to the in-depth from the surface for both specimens in order to assess the complete residual stress field produced by the shot-peening treatment. Material was removed by controlled chemical attack. The residual stress relaxation due to material removal was compensated and corrected according to the standard[51] by means of Moore & Evans technique [52]. Obtained values of each in-depth measurement for machined and SP samples are shown in Table 7. Graphic representations of the initial residual stress fields are presented in Fig. 6. Machined samples show on the surface tensile stresses in both directions. These stresses reduce to zero in a depth near to 10–20 μm, and then, turn into the compressive direction. Compressive and tensile peaks can be considered with the same magnitude level, with the compressive maximum being quite a lot higher. The extension of the compressive stress field is up to 0.2 mm in depth, however, after 0.1 mm the stress level could be considered almost null.

It is easily appreciated what the effect of the applied shot-peening treatment is on the initial tensile stresses at the surface and the near-surface. They turn into compressive stresses with higher magnitude and higher extension. The maximum stress for transversal direction is located on the sub-surface (0.07 mm depth). However, this stress maximum has a similar magnitude as the measurement on the surface. Thus, the profile of the obtained residual stress field resembles a step function. This shape is usual for hard martensitic steels treated with a shot-peening with medium-low Almen intensity [53]. Higher shot-peening intensities lead to a displacement of the maximum peak to the interior of the sample and an extension of the compressive field [9 16] Other mechanical treatments introduce compressive residual stress fields with higher magnitude, higher deeps and with a smoother reduction gradient. Such mechanical treatments are LSP [29] and treatments with burnishing process [54] or LPB [41].

In the same way as with the surface, it is not presented as a complete equi-biaxiality on the magnitude of main stress components. The transversal component possesses a slightly higher magnitude. The residual stress field extends up to a depth close to 0.18 mm. After this depth, a very low magnitude tensile stress area is found. This is due to the wide longer unaffected area that lies along the depth on the cross-section [28]. This tensile stress area is generated to keep the internal loads balanced within the sample. Fig. 5, also presents the extension of this residual stress field along the complete circumference of the mid-plane of the sample. This extension identifies an area of the material, located on the external ring, with a depth close to 0.18 mm. This area, on

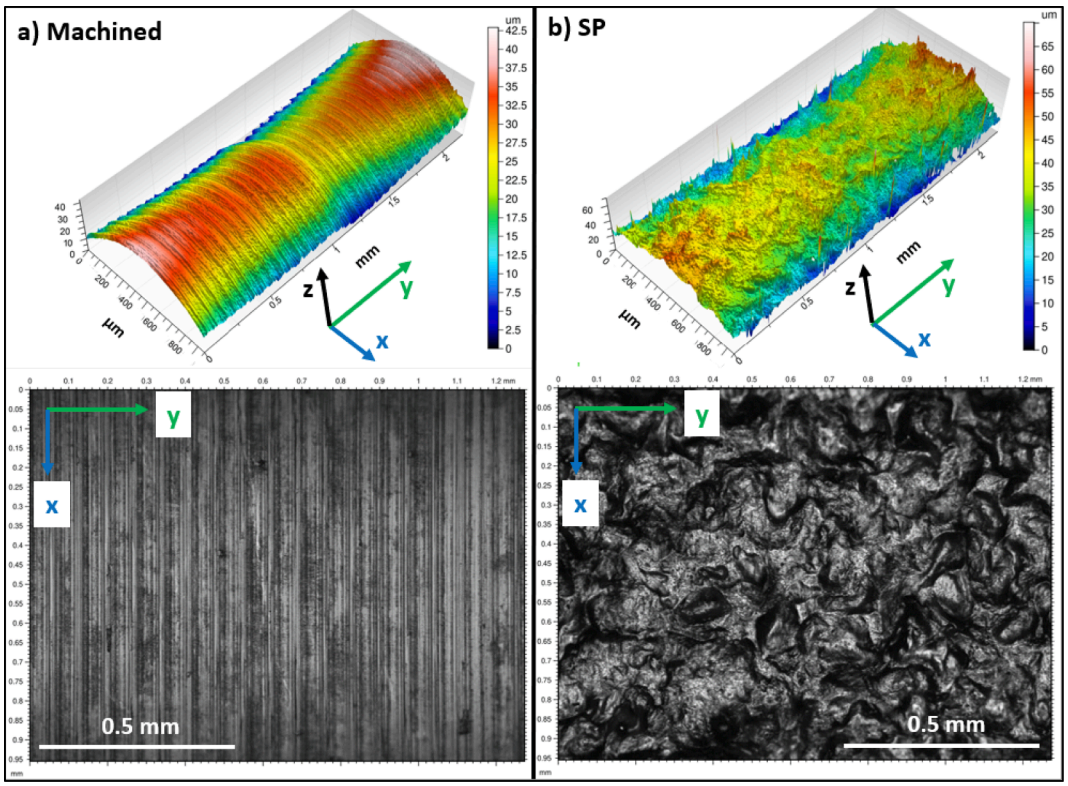

Fig. 4. The 3D topography and surface detail of specimens: (**a**) machined and (**b**) SP.

Table 5
Roughness measurements (Ra and Rz).

	Ra (μm)	Rz (μm)
Machined	0.81	4.50
Polished [42]	0.03	0.18
SP	1.93	11.3

the external ring, represents around about 6% of the total surface of the cross-section. This ring is the area mechanically affected by shot-peening treatment. The other area, which is the core, remains almost in the same way as a non-treated specimen.

2.6. FWHMa

FWHM (full width of the diffraction peak at half maximum intensity) is a parameter obtained by means of the XRD technique and it was evaluated using the peak-fit option of the WinPLOTR software. It quantifies the so-called type II micro-strains and dislocation density modifications, the crystal size and includes the instrumental (IRF) broadening [11]. FWHM represents the cold-work introduced on the specimen (sub-)surface due to each hit from the shots during the shot-peening process. After a mechanical treatment application like shot-peening, this parameter tends to increase from the value associated with the base material. Thereby exhibiting the material micro work-hardening properties due to the increase of distortion and dislocation quantities.

Measurements obtained on the surface for machined and SP samples are shown in Table 8. On the surface, FWHM presents a higher value for the non-treated specimen [13]. In some Q + T steels, this parameter tends to reduce its value due to a material work-softening tendency [55]. Nevertheless, this reduction is not so significant and it is related with the low intensity of the shot-peening treatment.

The measurements were extended to in-depth. Results are presented in the Fig. 7. The FWHM value associated to the base material is-0.41° and this value is related with hardness and tempering temperature of the steel [20]. For the SP samples, the depth of affected layer, until achieve the base material associated value, is-0.18 mm. This depth is in accordance with the depth of hardness increase and the extension of the compressive residual stress. For as machined samples, the reduction of the FWHM parameter till achieve the reference value is steeper. The FWHM value on the surface increases a 35% from its base material value for SP samples and a 56% for as machined samples.

3. Experiments and background

In this work, all tests were performed in the Lab. of Mechanical Engineering Department of the Faculty of Engineering UPV/EHU (Bilbao, Spain) with a servo-hydraulic test rig 8805 MTB (100 KN) manufactured by Instron (High Wycombre, UK). Tests were performed at room temperature with quasistatic or cyclic axial loading, conducted under stress applied (load) control, without an accuracy sample's strain control.

3.1. Axial fatigue tests

From an engineering point of view, it is of interest to evaluate fatigue

Table 6
Average initial residual stress tensor for SP samples (MPa).

σ_{xx}	σ_{yy}	σ_{zz}	τ_{xy}	τ_{yz}	τ_{xz}	σ_1	σ_2	σ_3
−660.3	−528.6	0.0	106.8	−9.0	60.1	−727.0	−468.3	6.3

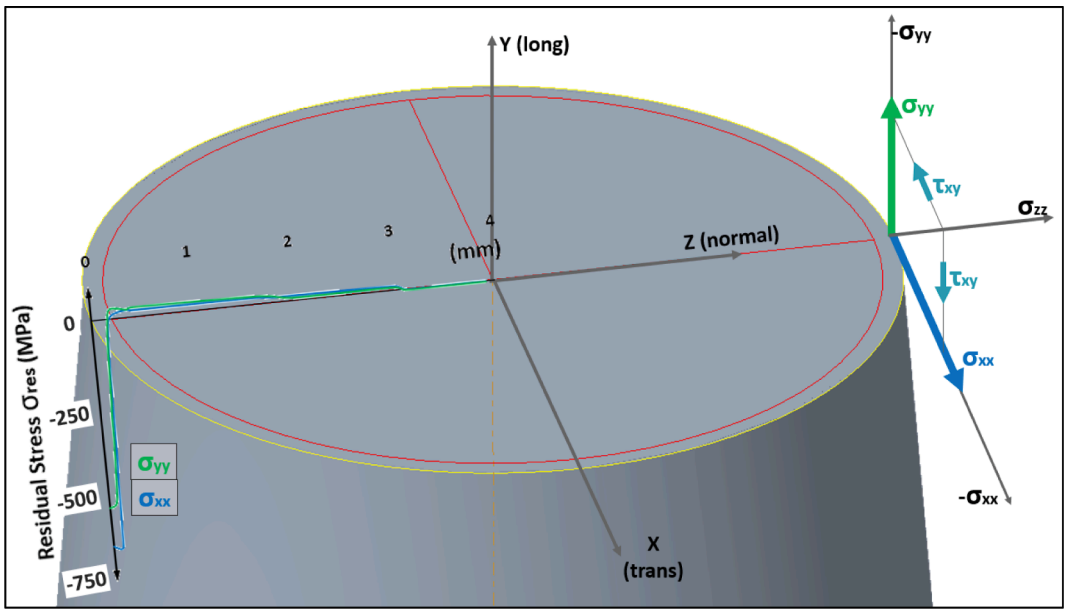

Fig. 5. Residual Stress components on the specimen.

Table 7
In-depth longitudinal & transversal residual stress of machined and SP samples.

Machined			Shot-peened		
depth (mm)	σ_{xx} trans. (MPa)	σ_{yy} long. (MPa)	depth (mm)	σ_{xx} trans. (MPa)	σ_{yy} long. (MPa)
0.000	56 ± 14	185 ± 9	0.000	−651 ± 6	−537 ± 5
0.014	81 ± 6	−128 ± 3	0.069	−693 ± 6	−483 ± 4
0.033	−177 ± 5	−212 ± 4	0.091	−654 ± 4	−434 ± 4
0.068	−120 ± 4	−91 ± 2	0.105	−533 ± 5	−353 ± 4
0.098	−78 ± 3	−47 ± 4	0.118	−406 ± 4	−235 ± 5
0.199	−26 ± 4	−18 ± 7	0.152	−47 ± 4	−14 ± 8
0.395	30 ± 6	−26 ± 5	0.365	23 ± 5	32 ± 4

improvement generated by SP treatment compared to a non-treated (as machined) state. A batch of cyclic tests were developed to determine the S-N curves of machined and SP samples.

Due to the limited number of specimens available, especially with machined samples, the selection of load-cases was supported according to [56]. Hourglass shape of the testing samples tends to concentrate the crack initiations and failures in a restricted area of the specimen, close to the mid-cross section. Thus, scatter is significantly limited [57].

Axial sinusoidal external stresses (loads) applied had no mean stress (R: −1) and frequencies were selected from 5 to 20 Hz. The S-N curve knee for this type of steel is frequently located bellow 10^6 cycles. Therefore, run-out was set at 1.5×10^6 cycles. In previous investigations, similar comparison data between machined and SP samples were studied under rotating bending fatigue [41]. Besides, the axial R: −1 fatigue S-N curve for polished specimens were calculated [42].

3.2. Quasi-static tests

Axial quasi-static tests were carried out with same set-up and test rig, with SP samples, in order to evaluate the surface residual stress relaxation under quasistatic loads. The aim of these tests was to evaluate the influence of applied stress directions (compressive or tensile) and their magnitude. Defined quasi-static tests consisted of two half cycles; one with tensile stress applied and the other one with compressive load, both with the exact same magnitude. So, according to the sequence of load application, two types of quasi-static test are defined: 1. tensile + compression (T-C) and 2. compression + tensile (C-T). Each half cycle is composed of three steps:

- 30 s with an increasing load ramp with constant slope till achieve specified load (stress)
- A plane step of 5 s maintaining the load (stress) constant
- 30 s for decreasing load ramp with constant slope till unloading the specimen

Both the completed quasi-static tests (T-C & C-T) can be seen in Fig. 8. They have similar appearance as a sinusoidal load, which is characteristic of cyclic testing. Before and after each half cycle (points 0, 1 and 2, in Fig. 8) residual stress on the surface of each sample was measured. Six different applied stress magnitudes were defined, whose test data can be seen in Table 9.

The stress applied magnitude for tests n° 4 was selected with the same magnitude as the monotonic yield point (1084 MPa) in order to achieve the onset of plastic strain. This is the main mechanism for residual stress relaxation [16]. In addition, for tests n° 5 and 6, the stress applied exceeds the yield point. The other three tests were performed with lower stress magnitudes than the monotonic yield point. Two of them correspond to the selected stress applied range for cyclic loading. The aim of this selection is to notice the differences between static and cyclic relaxation processes.

3.3. Cyclic relaxation tests

Axial sinusoidal cyclic tests were carried out with the same set-up as previous mentioned tests with SP samples, in order to evaluate the surface residual stress relaxation under cyclic loading against the number of cycles performed (N). With the initial residual stress tensor measured on the surface of a SP sample, the test procedure consisted of applying a defined number of cycles of the external stress. Then, the specimen was removed from the test rig and the surface residual stresses were measured by means of XRD. This process was repeated until the specimens achieved their fatigue failure.

Evaluation of the residual stress is only focused on the surface of the samples in order to use the same specimen for each test. The value on the surface is representative of the residual stress field presented in Fig. 6. With the progress of the relaxation process, the magnitude and the depth of the stress field are seen to be gradually reducing. This reduction, on the magnitude and the depth of the stress field, will be proportional to

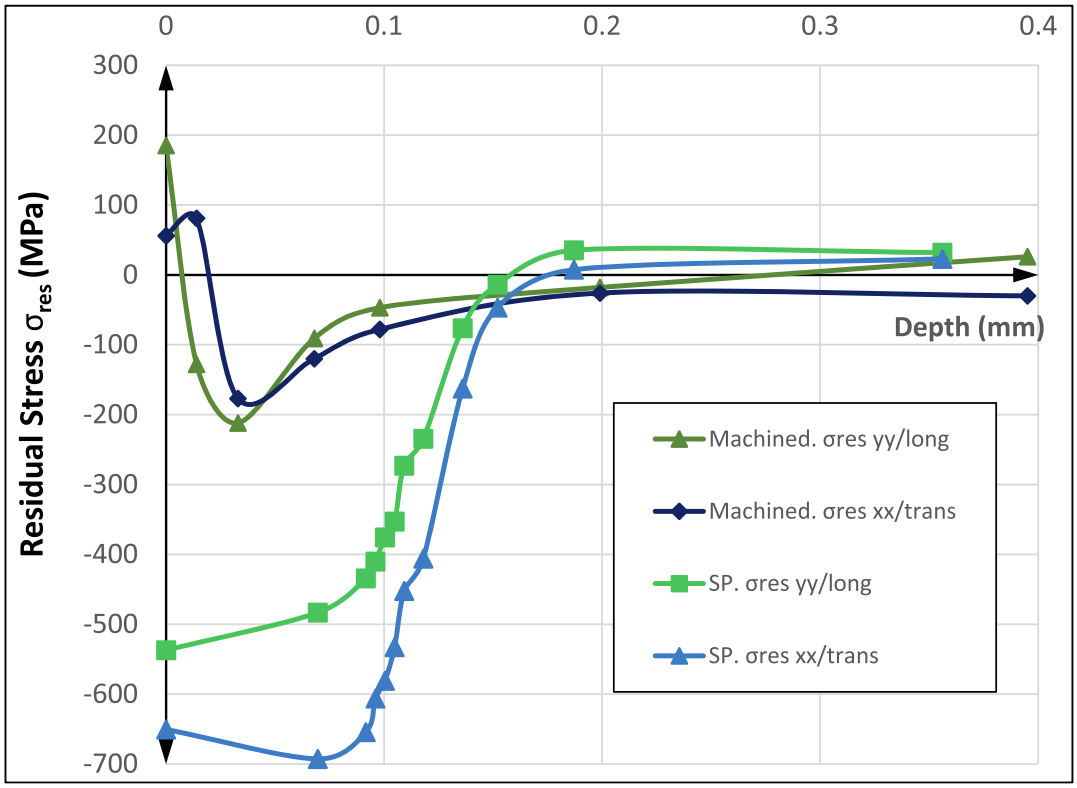

Fig. 6. In-depth residual stress field in machined and SP specimens.

Table 8
FWHM measured values.

Specimen	FWHM [°]	Peak Pos. [°]
Machined	0.642	68.352
SP	0.553	68.348

the amplitude of the applied stress [53].

Alternating stress applied (σ_a) had no mean stress (R: −1), the frequency was set at 5 Hz and four different stress magnitudes were selected. Two selected stress levels were ± 849 MPa and ± 703 MPa, which were the same as previous research with rotating bending fatigue cycles [41]. The other two stress levels were set at ± 776 MPa, which is the average stress level between the first two mentioned levels, and ± 630 MPa. The stress step between each four stress levels is 73 MPa.

With these four stress levels selected, the complete fatigue range is covered. The highest applied stress level can be considered a LCF fatigue case, where plastic deformation has the main role in contributing to failure. A close case, near the LCF limit, can be considered for the second highest stress level, ±776 MPa. On the other side, the lowest applied stress level has a magnitude lower than fatigue limit (see section 4.1), where main strain is elastic. For this point, the test finishing criteria was considered at 10^6 cycles.

Table 10 shows the main data for cyclic tests, including the estimated values of total, elastic and plastic strain for each stress level, calculated from [45] by means of the equation Mean Stress Effect on the Axial Fatigue Strength (Eq. (1)) proposed by Ramberg & Osgood [58]. These strain values provide a clear vision of the stress-strain status at each stress level proposed. As mentioned before, the material used in this research has slightly higher mechanical properties. Hence, the plastic strains presented will be quite lower than calculated. The coefficient "r" is the ratio of plastic strain against the total strain and *N* is the number of cycles of fatigue life.

$$\varepsilon_a = \varepsilon_{a,e} + \varepsilon_{a,p} = \frac{\sigma_a}{E} + \left(\frac{\sigma_a}{K'}\right)^{1/n'} \quad (1)$$

4. Tests results

4.1. Axial fatigue performance

The S-N curves for both types of samples are calculated according to ASTM E739-10-2015. Fatigue limit is calculated by the *staircase method* with a stress step of 9 MPa. Fatigue curves are presented in Fig. 9. Table 11 displays the main data describing the three fatigue curves.

The Basquin [59] equation related to R: −1 axial fatigue tests can be expressed in the next way:

$$\sigma_a(N) = \sigma_0 \cdot N^{-\frac{1}{m}} \quad (2)$$

where $\sigma_a(N)$ is the variable stress amplitude, *N* is the number of cycles of fatigue life, and *m* and σ_0 are Basquin parameters for S-N curves. These are obtained according to data results of the tests (see Table 11). The following equations for machined and SP specimens can be expressed:

Machined:

$$\begin{array}{ll} 10^4 \le N \le 2.7\cdot10^5 & \rightarrow \sigma_a(N) = 3501.45\cdot N^{-0.15219} \\ N > 2.7\cdot10^5 & \rightarrow \sigma_a(N) = 522 \end{array} \quad (3)$$

Shot-Peened:

$$\begin{array}{ll} 10^4 \le N \le 6.2\cdot10^5 & \rightarrow \sigma_a(N) = 1391.04\cdot N^{-0.05851} \\ N > 6.45\cdot10^5 & \rightarrow \sigma_a(N) = 636 \end{array} \quad (4)$$

As can be directly seen with the S-N curves represented in Fig. 9, the SP specimens show an improvement of 21.8% (+114 MPa) in the R: −1 axial fatigue limit, as to those compared with machined specimens. Furthermore, the SP axial fatigue limit is slightly higher (+3.4% or + 21 MPa) than the mirror polished axial fatigue limit, which provides an increment of 17.7% compared to the machined fatigue limit. This improvement is only related with the mirror finish of the surface. Thus,

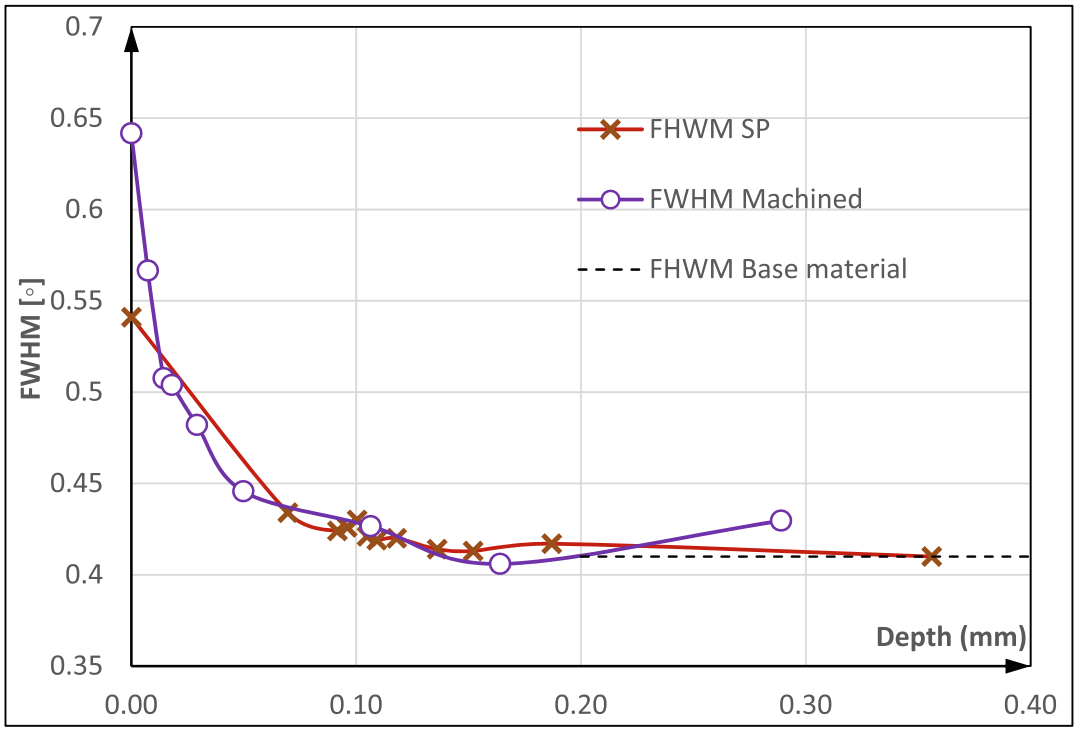

Fig. 7. FWHM for machined and SP specimens.

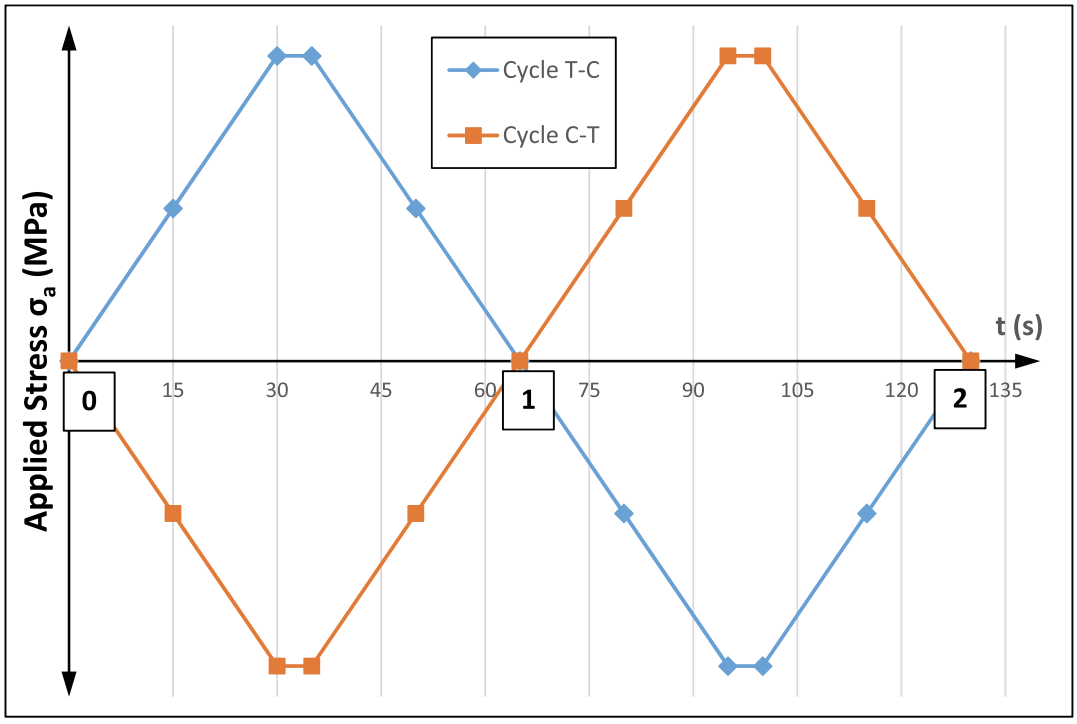

Fig. 8. Quasi-static tests definition: T-C & C-T.

the next improvements factors for SP treatment can be introduced:

$$i_{SP} = \frac{\sigma_{-1\,SP}}{\sigma_{-1mac}} = \frac{636}{522} = 1.218 \quad i'_{SP} = \frac{\sigma_{-1\,SP}}{\sigma_{-1}} = \frac{636}{615} = 1.034$$

Rotating bending and R: −1 axial fatigue S-N curves for Q + T DIN 34CrNiMo6 in the status of machined, mirror-polished and SP are already calculated. Fatigue limits for each case are presented in Table 12.

Compared to mirror-polished specimens, SP samples show an improvement on fatigue performance higher for axial fatigue (+21 MPa) than for rotating-bending (+0 MPa). Same relation was shown in the study [19].

Table 9
Quasi-static load tests definition.

Test Name	Max. stress in 1st half-cycle (MPa)	Max. stress in 2nd half-cycle (MPa)	Stress (load) speed (±MPa/s)
T-C 1	630	−630	21
T-C 2	850.5	−850.5	28.34
T-C 3	978.2	−978.2	32.61
T-C 4	1084.0	−1084.0	36.13
T-C 5	1118.9	−1118.9	37.29
T-C 6	1153.8	−1153.8	38.46
C-T 1	−630	−630	21
C-T 2	−850.5	850.5	28.34
C-T 3	−978.2	978.2	32.61
C-T 4	−1084.0	1084.0	36.13
C-T 5	−1118.9	1118.9	37.29
C-T 6	−1153.8	1153.8	38.46

Table 10
Cyclic test main data.

Test Name	σ_a (MPa)	N	ε_a (%)	$\varepsilon_{a,e}$ (%)	$\varepsilon_{a,p}$ (%)	$r = \varepsilon_{a,p}/\varepsilon_a$
M1	± 849	4890	1.021	0.412	0.609	59.7%
M2	± 776	17,467	0.596	0.377	0.219	36.8%
M3	± 703	100,433	0.413	0.341	0.071	17.3%
M4	± 630	10^6	0.326	0.306	0.021	6.3%

4.2. Quasi-static relaxation

External stresses applied are axial, along the longitudinal axis. So, the main component of the residual stress field that receives greater relaxation is the longitudinal component σ_{yy}. For this reason, this component is considered for the relaxation study. Data obtained from quasi-static tests is presented in Table 13 and displayed in Fig. 10. Initial residual stress (point 0) and residual stress after each half cycle (points 1 and 2) are presented. Three direct observations regarding presented results are the followings:

- The amount of stress relaxed is directly proportional to the applied stress magnitude.
- Compressive applied stress generates higher stress relaxation than tensile applied stress.
- Tensile applied stress generates stress relaxation when its magnitude is higher or equal to the monotonic yield point. If its magnitude is lower than the yield point, it produces no relaxation or even increases the residual stress magnitude [18].

Measurements of FWHM are presented in Table 14 and do not show a direct interpretation [60]. In general terms, after a tensile half cycle, the FWHM parameter tends to decrease its value and after a compressive test, it tends to slightly increase.

4.3. Cyclic residual stress relaxation

The residual stress tensor on the surface is obtained after each set of cycles for the four tests. All the stress components tend to reduce during cyclic loading. However, the cyclic loading is axial, so the main component that receives greater relaxation is the longitudinal σ_{yy}. For this reason, this component is considered for the relaxation study.

Evolution of the surface residual stresses for the four different stress levels are presented together in Fig. 11 and the data is shown in Table 15. Lines presented for each stress case correspond to the least

Table 11
Relevant data defining the axial fatigue S-N curves.

	Machined	Polished [42]	SP
N_g (cycles)	10^4	10^4	10^4
σ_g(MPa)	862	840	811.5
N_e(cycles)	$2.7{\cdot}10^5$	$6.23{\cdot}10^5$	$6.45{\cdot}10^5$
σ_{-1}(MPa)	522	615	636

Table 12
Obtained fatigue limits for Q + T DIN 34CrNiMo6.

Type of Load	Machined	Polished	SP
Rot. bending	$\sigma'_{-1mac} = 465$ MPa	$\sigma'_{-1} = 645$ MPa	$\sigma'_{-1SP} = 645$ MPa
Axial	$\sigma_{-1mac} = 522$ MPa	$\sigma_{-1} = 615$ MPa	$\sigma_{-1SP} = 636$ MPa

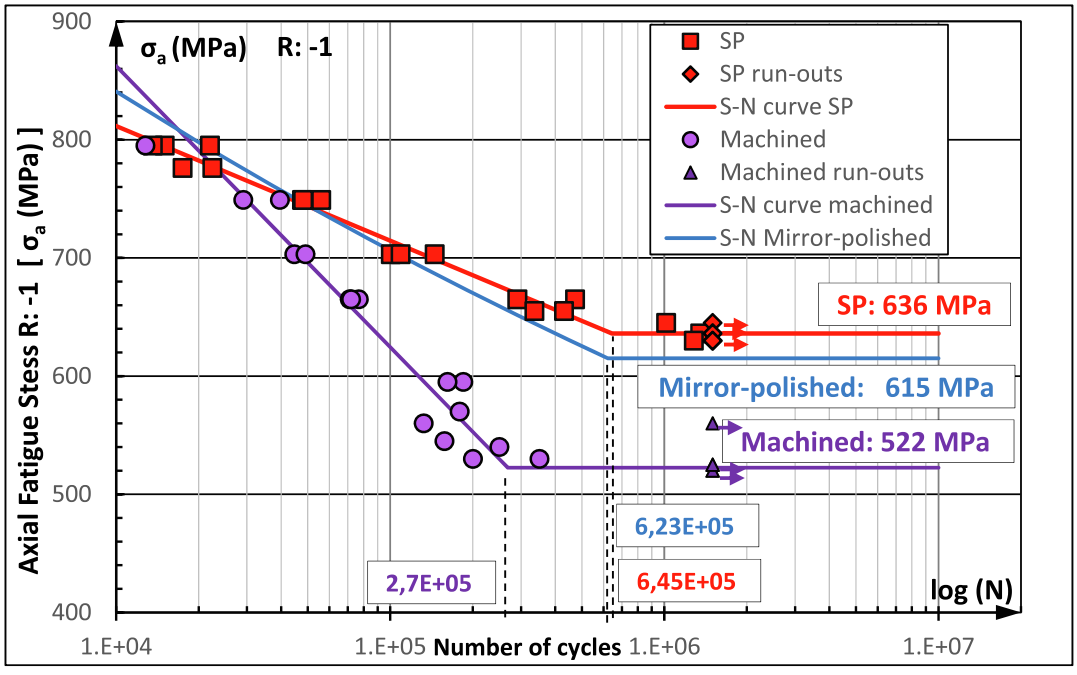

Fig. 9. R_{-1} Axial Fatigue S-logN curves of machined and SP specimens.

Table 13
Quasi-static Load tests results. $\sigma_{res\ yy}$ in MPa.

	T-C 1	TC-2	T-C 3	TC-4	TC-5	TC-6	C-T 1	C-T 2	C-T 3	C-T 4	C-T 5	C-T 6
σ_{res} **0**	−544.1	−533.4	−533.8	−525.2	−536.7	−535.0	−545.2	−544.1	−526.0	−536.4	−534.9	−530.9
σ_{res} **1**	−564.9	−559.2	−555.3	−393.8	−299.1	−213.5	−449.4	−284.1	−250.2	−169.6	−157.8	−125.0
σ_{res} **2**	−438.3	−376.5	−196.2	−172.4	−109.1	−62.8	−450.4	−341.2	−333.2	−184.8	−141.8	−125.3

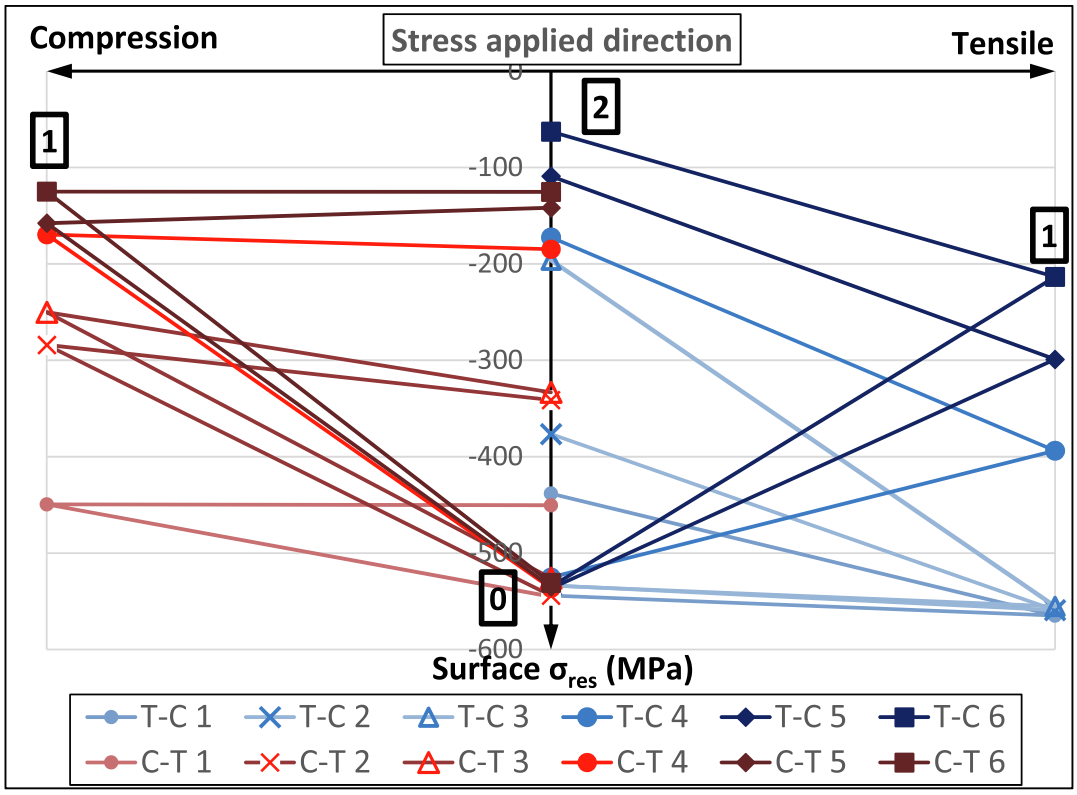

Fig. 10. Stress Relaxation after T-C & C-T quasi-static tests.

Table 14
Quasi-static Load Tests FWHM measurements.

	T-C 1	T-C 2	T-C 3	T-C 4	T-C 5	T-C 6	C-T 1	C-T 2	C-T 3	C-T 4	C-T 5	C-T 6
0	0.538	0.537	0.540	0.590	0.537	0.551	0.543	0.540	0.540	0.577	0.570	0.547
1	0.541	0.541	0.538	0.559	0.528	0.542	0.533	0.547	0.537	0.578	0.572	0.545
2	0.540	0.545	0.536	0.580	0.542	0.543	0.538	0.543	0.523	0.557	0.547	0.515

square fitting of the data presented.

With these test data, there are three main conclusions that can be directly observed:

(1) The residual relaxation rate increases with the magnitude of the stress applied [61 19] or, in other terms, with the increase of plastic strain/deformations.
(2) An important stress relaxation occurs in the initial cycles.
(3) For the cases with higher stress applied (or higher plastic deformations) relaxation rate is *not-null* until the end of fatigue life. This means, that there is no stabilized residual stress level where residual stress converges. A typical equation observed in the literature is presented in (Eq. (5)). This stabilized residual stress can be found for the two lower stress levels.

$$\sigma_{est} \approx \sigma_{yp} - \sigma_{ap} \tag{5}$$

The surface residual stress relaxation under the same applied stress magnitude (±849 MPa and ± 703 MPa) for the same material and the same SP process, under rotating bending fatigue [41] and under axial fatigue (R: −1) is already evaluated. In Fig. 12, the residual stress measurements, in the Von Misses equivalent stress, can be easily noticed. The straight lines for axial fatigue relaxation tendency have a steeper slope than rotating bending cases and the final surface residual stress level for axial loading is lower than for rotating bending. So, it can be concluded that with the application of axial stress, a higher relaxation rate generated, due to the different stress gradient [18 19 24].

Stress generated on the cross-section due to rotating-bending test has a gradient. Stress distribution reduces its magnitude from the surface (maximum) to the centre (null). However, axial loading generates the maximum stress on the complete cross-section, so:

– For axial loading, higher plastic strains are generated on the complete core, which favours the residual stress relaxation according to (Eq. (12)), from the core to the external ring.

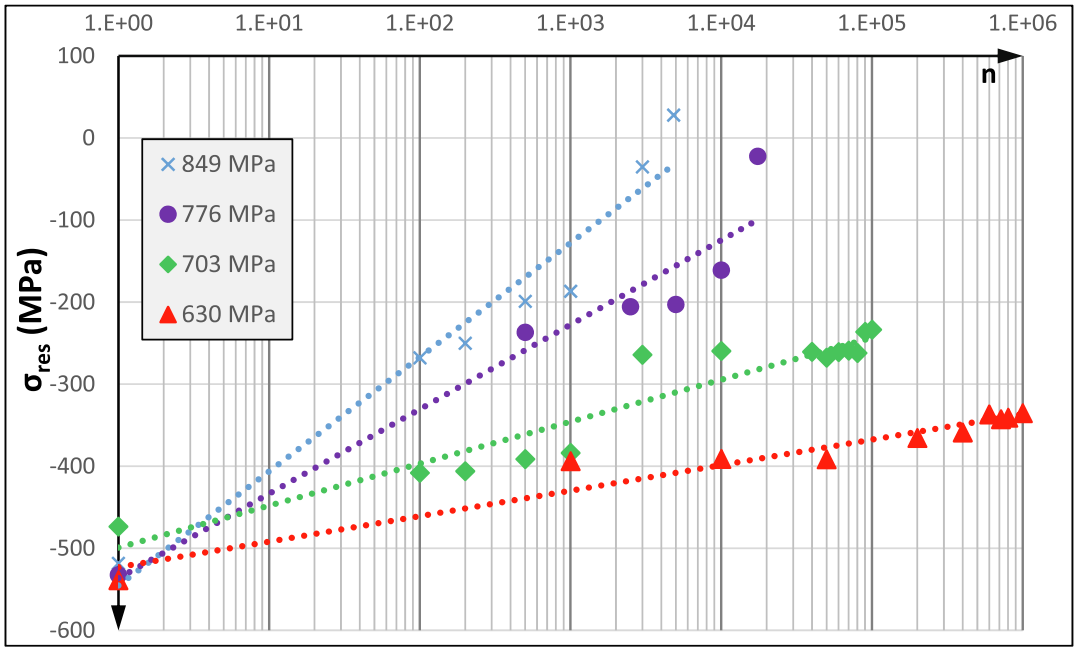

Fig. 11. Surface residual stress relaxation for four stress levels.

Table 15
Surface residual stress (MPa) evolution with number of cycles.

M1: ± 849 MPa		M2: ± 776 MPa		M3: ± 703 MPa		M4: ± 630 MPa	
n	$\sigma_{yy\ res}$	n	$\sigma_{yy\ res}$	n	$\sigma_{yy\ res}$	n	$\sigma_{yy\ res}$
0	−518.2	0	−532.3	0	−473.4	0	−538.8
100	−267.8	500	−236.8	100	−407.9	1000	−393.8
200	−250.0	2500	−205.6	1000	−383.8	50,000	−391.5
500	−198.9	5000	−202.8	10,000	−259.5	200,000	−365.5
1000	−186.8	10,000	−161.1	50,000	−267.7	400,000	−358.8
3000	−35.1	17,447	−22.4	80,000	−261.9	800,000	−340.8
4823	28.0			100,000	−233.4	1,000,000	−335.3

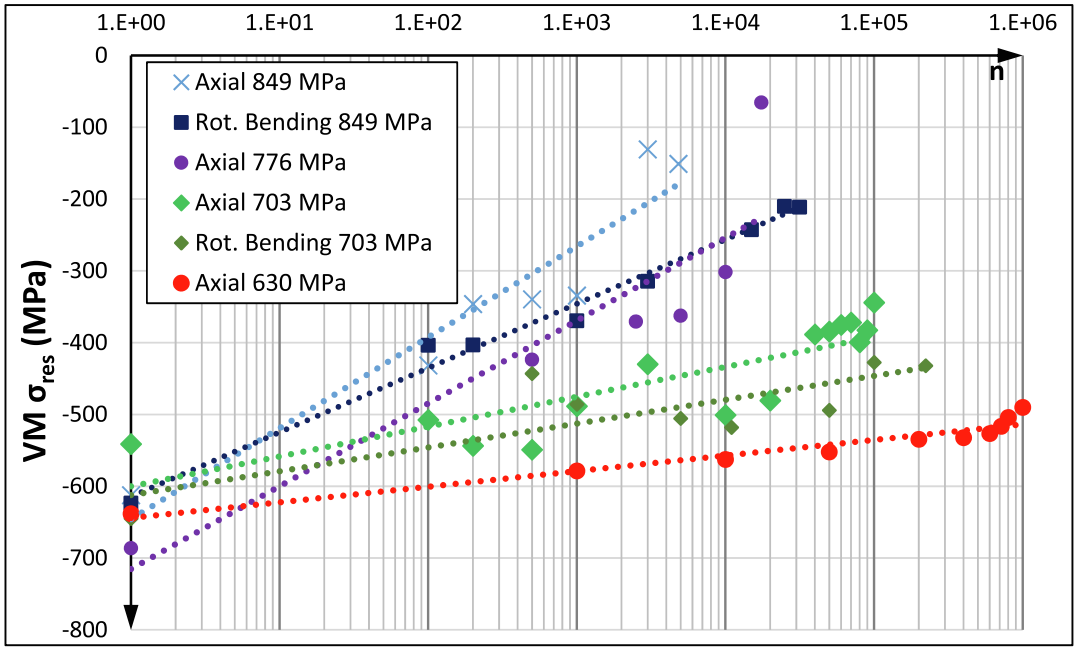

Fig. 12. Surface residual stress relaxation.

– As can be seen in the Fig. 14, on the external treated ring area, the complete area achieves the maximum stress, increasing the plastic strain generated while axial fatigue testing.

5. Fractographic analysis

Rupture cross-section images are taken for the three specimens that suffer breakage (M1, M2 and M3) after the cyclic relaxation tests, with the aim of studying the place of crack initiation and propagation, under the different applied stress levels. In order to provide a better analysis of the effect of shot-peening on crack growth and propagation, these three SP specimens are compared with machined specimens at similar stress levels, used in the tests for the elaboration of the S-N curve. In general, no novel conclusions are observed with respect to previous investigations [62].

In Fig. 13 **a)**, **b)** and **c)**, it is observed that SP specimens show multiple crack initiation points on the surface and the quantity of cracks increases with the applied stress level increases. At higher levels of applied stress, crack propagation and crack growth are more abrupt. Fig. 13 **c)** shows the fracture section of the SP specimen with the lowest applied stress (703 MPa) which presents, five different zones of crack propagation. In the case of the machined specimens, the number of crack initiation points is drastically reduced and most of them are located on the surface. Crack propagation traces in these machined specimens are clearly observed.

6. Results analysis and discussion

6.1. Axial fatigue improvement

The two main effects produced by the SP treatment on the specimens are the introduction of residual compressive stress field and the deterioration of the surface roughness. The introduction of compressive residual stress field provides an improvement on fatigue life, due to the reduction of crack growth rate [63]. In contrast, the deterioration of surface roughness reduces the fatigue strength due to the susceptibility of stress concentration factors and greater possibilities of crack initiation [53]. In this campaign of R: −1 axial fatigue tests, the worsening of surface integrity (compared to mirror-polished surface) does not play as great a role on the fatigue performance than compressive residual stresses.

This consideration can be quantified by means of Marin's coefficients [64]. Using the values for the R: −1 axial fatigue limits for polished and SP samples, the coefficient C^{e}_{SP} can be calculated. C^{e}_{SP} includes the coefficients related to the surface finish $C_{sur\ SP}$ and the mechanical treatment applied $C^{e}_{mec\ SP}$ (Eq. (6)).

$$C^{e}_{SP} = \frac{\sigma_{SP}}{\sigma_{-1}} = 1.034 \;\; C^{e}_{SP} = C^{e}_{surSP} \cdot C^{e}_{mecSP} \tag{6}$$

The surface finish coefficient can be estimated from the Johnson data-sheet [65 66] by means of tensile strength σ_{ut} and the surface roughness, Ra = 1.93 μm. Then, the coefficient $c_{sur\ SP}$ is approximately 0.8. Therefore, the coefficient related with the SP mechanical treatment, $C_{mec\ SP} \approx 1{,}29$ which fits properly with [67].

Once the fatigue limits are obtained for as machined, polished and SP specimens in the cases of rotating bending and R:-1 axial fatigue, the coefficients related to the load application gradient/case can be calculated and assessed. In the LCF limit, which is 10^4 cycles, the C^{g}_{t} coefficient can be stated as equal to 0.83 and for the fatigue limit, the estimated value of C^{e}_{t} coefficient is 0.9 [66–68]. Both coefficients also provide a verification that the testing axial load is applied in perfect alignment with the central axis and there is no generation of a bending load, which would be created by misalignment. The calculated coefficients for machined, polished and SP samples can be seen in Table 16. Polished and SP coefficients fit properly with the literature estimation and with experimental data. Nevertheless, the coefficient derived from the machined sample is slightly higher than theoretically expected. The as machined fatigue results showed a great dispersion, due to the surface roughness defined by tooling marks. In this case, the number of available samples was reduced and the fatigue limit obtained is quite higher than initially expected.

Finally, the "effective mean stress" σ^{ef}_{m}, introduced in previous works [40,69] for fatigue calculations, is presented in ((Eq. (7)). It is defined as a virtual or equivalent stress which is uniaxial, constant in time, with no

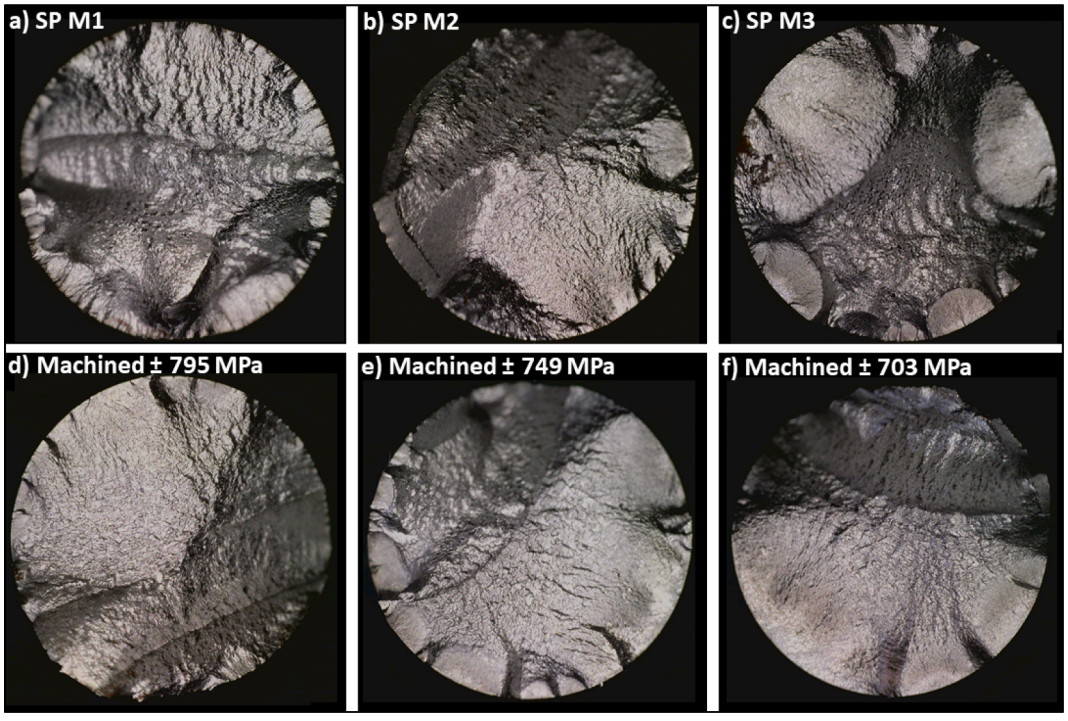

Fig. 13. Fracture section of SP samples (a, b & c) and machined samples (d, e & f).

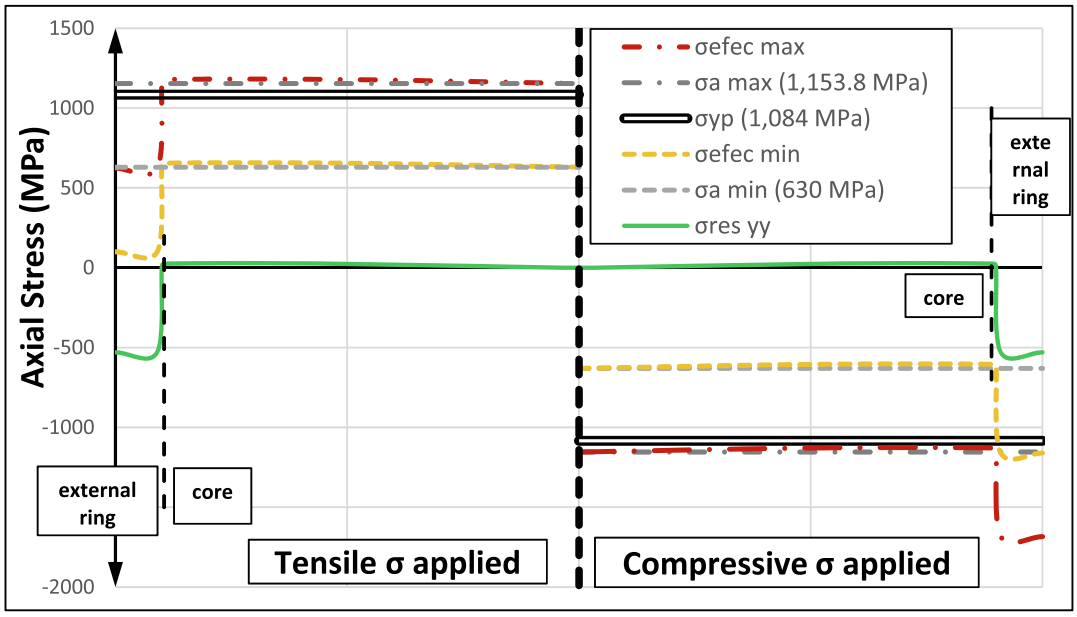

Fig. 14. Stress situation under external stress on the cross section of the sample.

Table 16
Load application coefficients for machined, polished and SP specimens.

Literature	Machined	Mirror-Polished	SP
$C_t^e = \frac{\sigma_e}{\sigma'_e} = 0.9$	$C_{tM}^e = \frac{522}{465} = 1.12$	$C_t^e = \frac{615}{645} = 0,95$	$C_{tSP}^e = \frac{636}{645} = 0.98$
$C_t^g = \frac{\sigma_g}{\sigma'_g} = 0.83$	$C_{tM}^g = \frac{862}{950} = 0.9$	$C_t^g = \frac{840}{950} = 0.88$	$C_{tSP}^g = \frac{811}{950} = 0.85$

gradient, causing the same effect in the fatigue strength (defined by means of the mirror-polished specimens) than a given mechanical treatment, which in this case is shot-peening.

From an engineering point of view, the fatigue strength improvement of SP process is usually compared with as machined samples. Therefore, $\sigma_m^{'ef}$ concept is also included in (Eq. (8)), which is defined by means of as machined fatigue limit, instead of the mirror polished limit.

Using the Dietmann criterion for including mean stresses, for the SP treatment:

$$\sigma_m^{ef} = \sigma_{ut} \cdot \left(1 - \left(\frac{\sigma_{-1\,SP}}{\sigma_{-1}}\right)^2\right) = 1209 \cdot \left(1 - \left(\frac{636}{615}\right)^2\right) = -84\ MPa \quad (7)$$

$$\sigma_m^{'ef} = \sigma_{ut} \cdot \left(1 - \left(\frac{\sigma_{-1\,SP}}{\sigma_{-1\,mac}}\right)^2\right) = 1209 \cdot \left(1 - \left(\frac{636}{522}\right)^2\right) = -586\ MPa \quad (8)$$

It is interesting to notice that value for $\sigma_m^{'ef}$ has a magnitude close to the residual stress on the surface generated by SP treatment.

6.2. Quasi-static relaxation interpretation

The main mechanism for residual stress relaxation is the appearance of plastic strains on the external ring area when compressive stress is applied. In this external ring area, which is affected by the residual compressive stress field, the *effective stress* can be defined as the sum of applied and compressive residual stresses. Therefore, plastic strains happen when this effective stress exceeds the monotonic yield strength $\sigma_{yp} = 1084$ MPa (Eq. (9)) [70]. This statement can be appreciated after all the compressive applied stress half cycles for T-C and C-T tests.

Secondary relaxation mechanism occurs from the core (internal area) of the sample, where no residual stress can be considered (small tensile residual stress exists in order to just maintain internal load equilibrium), if the applied stress (either tensile or compressive) exceeds the monotonic yield point, then, plastic strains will appear in this area. These plastic strains would relocate to the external ring, in order to maintain the mass and volume equilibrium, generating relaxation of the external compressive residual stresses (Eq. (10)) [71]. This can be appreciated in the first half cycle of T-C test n° 4, 5 and 6.

$$\text{External ring}: \quad \sigma_{yp} \leq -(\sigma_a + \sigma_{res}) \quad (9)$$

$$\text{Core of specimen}: \quad \sigma_{yp} \leq |\sigma_a| \quad (10)$$

These statements are better explained with the help of Fig. 14, where is represented a specimen middle cross section, under tensile applied stress (left side) and under compressive applied stress (right side). Data presented correspond to the developed tests, however, the intention is to provide a general explanation.

These explanations can be appreciated with quasi-statics tests n° 1, 2 and 3, where the magnitudes of applied stresses are lower than the monotonic yield point. In these three cases, compressive applied stresses produce surface residual stress relaxation proportional to the stress magnitude. However, the applied tensile stresses do not generate stress relaxation but also causes that compressive residual stress to increase. This increase can be related to residual stress measurement dispersion or with the appearance of tensile strains on the core which favours the compressive residual stress field due to a new internal stress/strain equilibrium situation [18]. This last fact also happens with second tensile half-cycle of C-T tests n° 3, 4 and 5.

According to the data of the test results presented in Table 13 it can be observed that T-C cycles produces higher stress relaxation than C-T cycles. This aspect is directly related to the effect of the tensile stress applied half-cycles. If they are applied after a compressive half cycle, they tend to increase the compressive residual stress magnitude. In the T-C, tensile cycles follow the tendency provided in (Eq. (10)).

6.3. Cyclic residual stress relaxation model

With the data of the surface residual stress relaxation, evaluated at four applied cyclic stress levels for SP samples, a model for predicting the relaxation process on the surface is proposed. This model considers three main factors.

1 – Plastic strains are the main mechanism for mechanical residual

stress relaxation. For cyclic loading, considering that this Q + T steel tends to cyclic-softening [46], the cyclic yield point is considered as the onset for plastic strains:

$$\sigma_{yp}\,(1084\,\text{MPa}) \rightarrow \sigma'_{yp}\,(825\ \text{MPa})\ \text{for cyclic loading}$$

$$\text{External ring}: \quad \sigma'_{yp} \leq |\sigma_a + \sigma_{res}| \tag{11}$$

$$\text{Core of the sample}: \quad \sigma'_{yp} \leq \sigma_a \tag{12}$$

2 – A higher magnitude of the sum of residual and applied stress introduces higher plastic strain, which favours higher relaxation rate. This coefficient, α, is related with the ratio r given in Table 10, where it is observed that the increase of plastic strain related to the higher applied stress:

$$\alpha = \left(\frac{\sigma_a}{\sigma'_{yp}}\right) \tag{13}$$

3 – In Fig. 11, it is observed that residual stress relaxation follows a logarithm reduction properly. A logarithmic factor proposes a higher relaxation rate in the initial cycles and then, this relaxation rate is gradually reduced along the total fatigue life. This approximation fits with data obtained.

$$\text{cycling factor} = \frac{\ln(n+1)}{\ln(N+1)} \tag{14}$$

where N is the fatigue life, which can be obtained from the presented Basquin equation for SP samples (Eq. (4)). Then, the proposed model for surface longitudinal stress relaxation for this SP steel is presented in the (Eq. (15)).

$$\sigma_{res}(n) = \sigma^0_{res} - (\sigma^0_{res} - [\alpha \cdot \sigma_a] + \sigma'_{yp})\frac{\ln(n+1)}{\ln(N+1)} \tag{15}$$

Fig. 15 presents a better explanation of the surface residual stress relaxation process, where a general description of the relaxation process is displayed with the help of tested data. In the lower region of the vertical axis, the external surface of the sample is shown. The upper region of the axis represents the core of the sample, which is without residual stress. In the initial cycles, if the sum of applied and residual stresses in the external ring area is higher than the yield point, the, an important compressive plastic strain appears, which produces a very high relaxation rate. The relaxation rate continually decreases with the reduction of the gap between yield point and stresses on the surface for both residual and applied. This stress reduction leads to a reduction of plastic strains. However, it must be considered that the yield point, for this Q + T steel, reduces with the number of cyclic loads applied, thereby increasing again the gap between stresses and promoting more plastic strains. This means that materials with cyclic-softening properties, will tend to generate greater residual stress relaxation [72].

In the proposed model (Eq. (15)), the cyclic yield point is set directly instead of using the monotonic yield point, which generally is set only for the first cycle. In the work presented in [46,47] with this same Q + T steel, stabilized hysteresis loops were achieved near 0.4 life ratio. So, in Fig. 15, a logarithmic decrease of the yield point in the initial cycles is proposed [19]. For an optimization of the proposed model, a study of the cyclic elastoplastic behaviour of this shot-peened steel, with constant

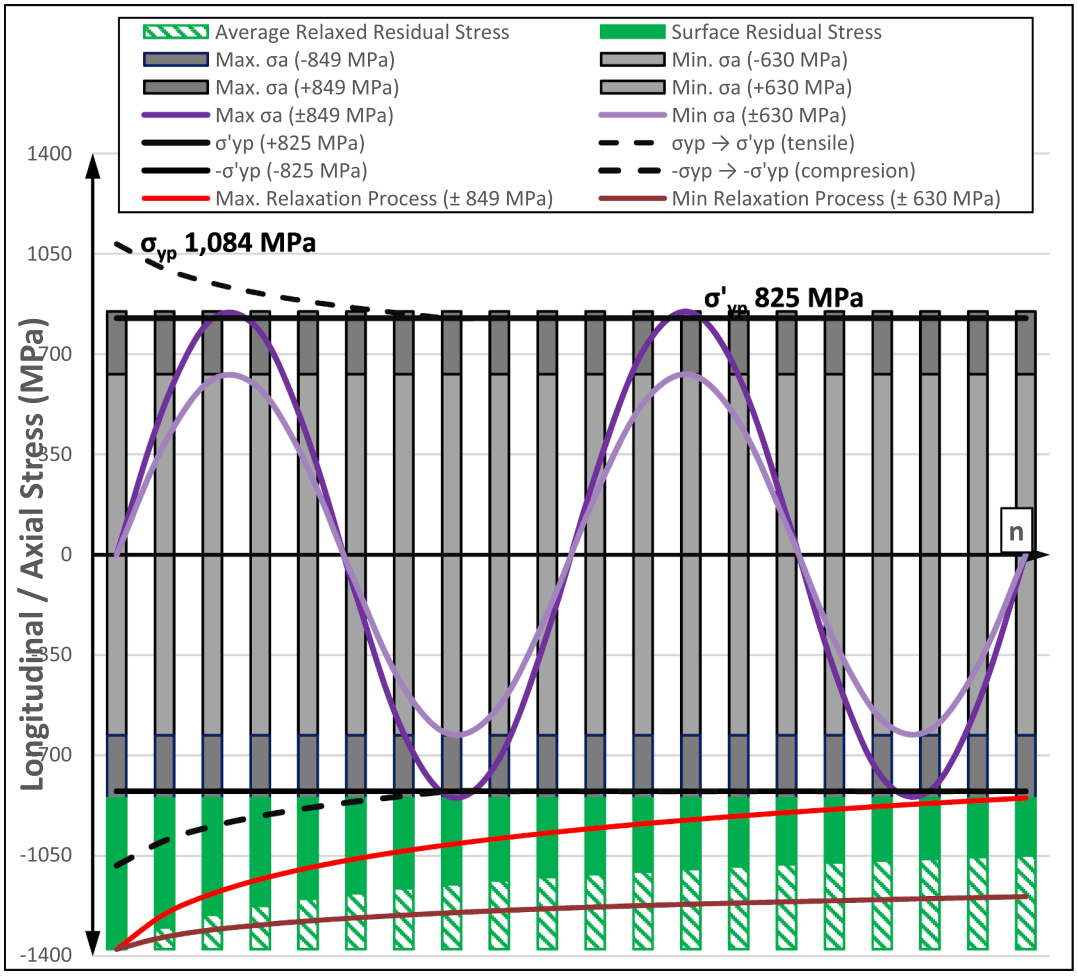

Fig. 15. Cyclic stress relaxation graphic.

amplitude cyclic stress applied and strain control, should be carry out [22]. However, in this actual research all of the test performed had to be conducted only as stress controlled. Another point that can be optimized in the model is the variation of the yield point on the external ring area due to cold-work introduced by the shot-peening treatment. In addition, the real compressive yield point could be checked because its magnitude is considered the same as in the tensile direction.

Finally, in the last stage of relaxation, if the applied stress is low and does not generate significant plastics strains by itself (see Table 10), the residual stress field achieves its stabilized value. After this point, surface residual stresses remain steady until the end of the fatigue life (Eq. (5)). The equation for stabilized residual stress can be expressed by means of (Eq. (16)).

$$\sigma_{est} = \sigma^{0}_{res} - \sigma_{relaxed} = \sigma^{0}_{res} - (\sigma^{0}_{res} - [\alpha \cdot \sigma_a] + \sigma_{yp}) \quad (16)$$

When the stress applied is high and by itself causes important plastic strain, both tensile and compressive, the relaxation process continues until the end of the fatigue life. Thus, the convergence of the residual stress to its stabilized value does not take place. The relaxation can be also promoted from the core of the specimen, when the applied stress produces plastic strains on this area.

The stress-case M1 with $\sigma_a \pm 849$ MPa is presented in Fig. 16. It can be deterministically seen an important initial residual stress relaxation, which gradually advances until the last cycle of failure. In the last cycles the residual stresses turn into the tensile direction. The FWHM parameter presents a continuous reduction for the whole progress of fatigue life. The reduction is more pronounced when there is higher residual stress relaxation rate. This reduction is related with the important plastic strains produced while testing and thus, the decrease of dislocation densities. At the end of the test FHWM almost achieves its value corresponding to the base material.

The stress-case M2 with $\sigma_a \pm 776$ MPa is presented in Fig. 17. Again, it can be appreciated an important initial residual stress relaxation, which advances until the last cycle of failure. However, in this case, the relaxation rate is lower, which could be considered close to setting a stage of convergence. The FWHM parameter presents a continuous reduction for the whole progress of fatigue life. However, in this case it is steadier. At the end of the test, FHWM approaches to its value corresponding to the base material. This lower reduction of the FWHM is related to the lower plastic strain development, and thus, with a less movement and a reduction of dislocations.

The stress-case M3 with $\sigma_a \pm 703$ MPa is presented in Fig. 18. It can be appreciated again that it is an important initial residual stress relaxation, but in this case, the relaxation rate is lower and *shorter* (considering the ratio n/N) than previous cases. In these initial cycles, where the relaxation rate is too high, the logarithmic model cannot properly follow the real relaxation progress. After these cycles, due to the low magnitude of the stress applied, the residual stress achieves its stabilized value, which remains almost steady for the rest of the fatigue life.

$$\sigma_{est} \approx \alpha \cdot \sigma_a - \sigma'_{yp} = -226\,\text{MPa} \quad (17)$$

The FWHM parameter only shows a variation in the initial cycles when the relaxation rate is too high. In this stage, important plastic strain is happening. After that, it remains almost constant for the complete fatigue process. This indicates that there is almost no plastic strain.

The stress-case M4 with ± 630 MPa stress applied is presented in Fig. 19. It can be appreciated that it is an initial residual stress relaxation, in the same way as previous stress-case. However, in this case the relaxation rate is a lot lower, and the logarithmic model properly represents the real data. After these cycles, residual stress achieves its stabilized value, which remains steady for the rest of the fatigue life.

$$\sigma_{est} \approx \alpha \sigma_a - \sigma'_{yp} = -344\,\text{MPa} \quad (18)$$

The FWHM parameter only shows a slight variation in the initial cycles when the relaxation rate is high. After that, it remains almost constant for the complete fatigue cycles tested. The complete stability of residual stress and FWHM, clearly indicates that there is almost no plastic strain.

7. Conclusions

Applied shot-peening generates, on the (near-)surface of the quenched and tempered DIN 34CrNiMo6 steel, a residual stress field with an average magnitude of −642.9 MPa (in terms of Von Misses equivalent stress) on the surface and it extends up to a depth of 0.18 mm. Furthermore, this shot-peening treatment produces a worsening of surface roughness, which is increased from a Ra 0.81 μm to 1.93 μm.

Due to the low-middle intensity of the applied shot-peening and the high hardness and resistance of this Q + T steel, only minor variations are generated in microstructure, hardness and the FWHM parameter.

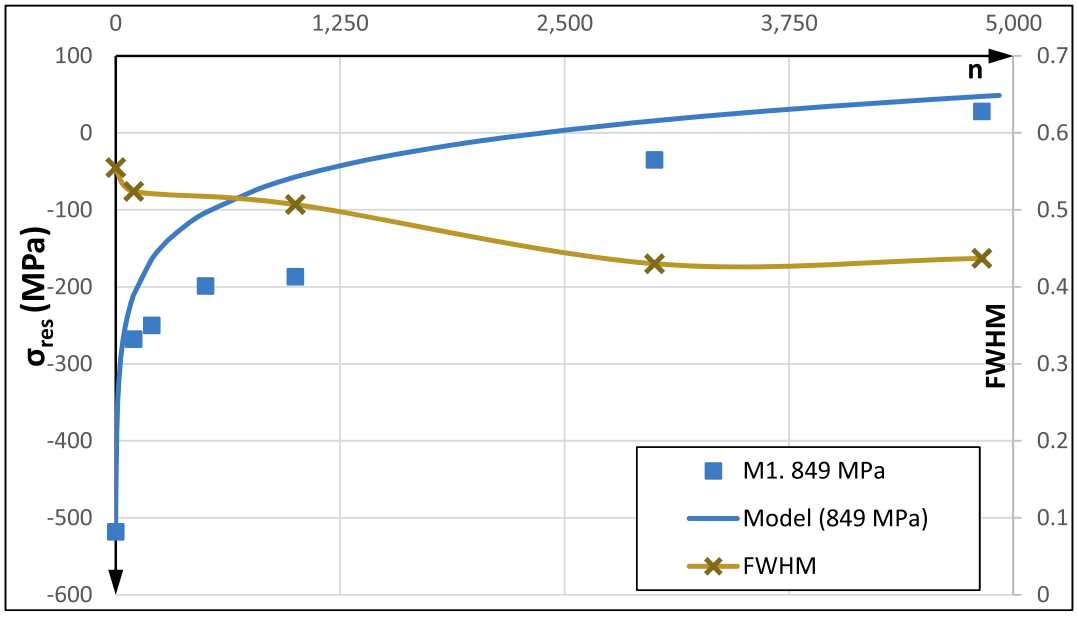

Fig. 16. Surface residual stress relaxation & FWHM for case M1. 849 MPa.

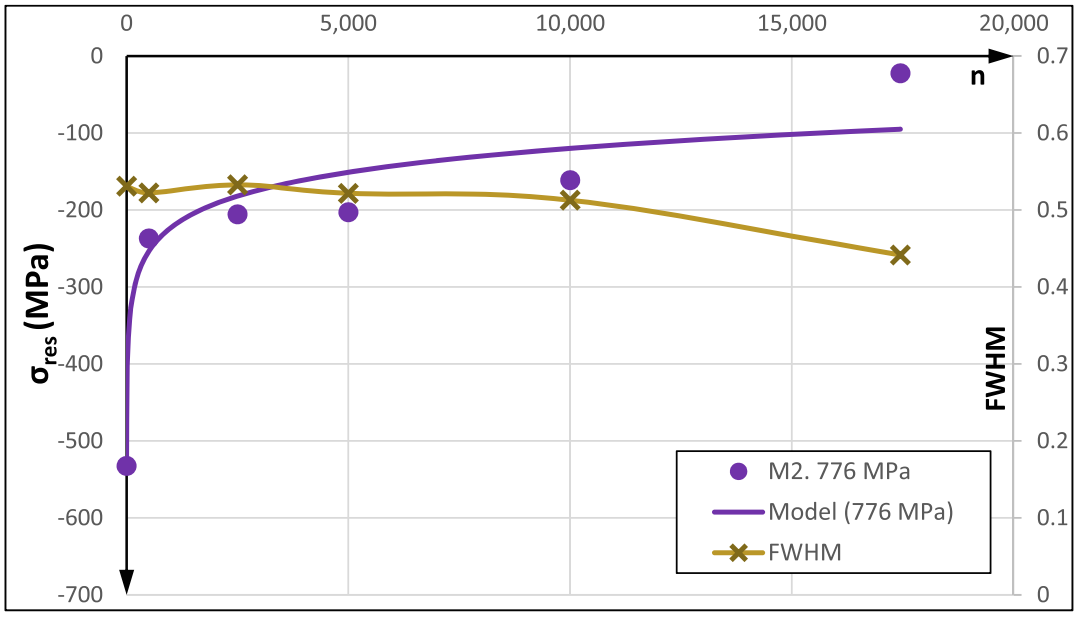

Fig. 17. Surface residual stress relaxation & FWHM for case M2. 776 MPa.

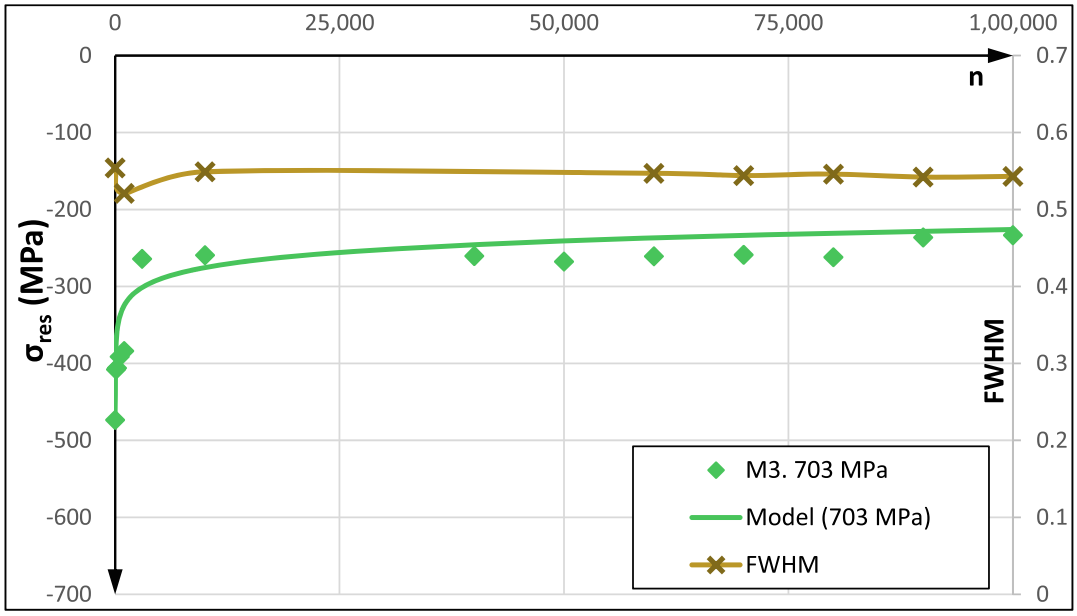

Fig. 18. Surface residual stress relaxation & FWHM for case M3. 703 MPa.

Material microstructure barely presents any variation and its hardness slightly increases, that is + 1.68 HRc (+4.4%) on the surface and along a depth with an extension like the residual stress field.

The FWHM parameter, which represent the crystallographic distortion, presents a value of 0.41° for the base material of the samples. On the surface of SP samples, the FWHM value increases up to 0.553°. The depth affected by the increase of the FWHM value extends to 0.18 mm, which is the same depth of the residual stress field and the increase of the hardness. However, on the surface, the parameter FWHM for as machined condition, shows a value of 0.642°. Consequently, the SP produces a reduction in the value of the FWHM parameter, related with the material work-softening tendency.

Despite the surface roughness deterioration, the R:-1 axial fatigue strength of SP samples increases compared to machined samples. This is due to the introduction of compressive residual stresses. The axial fatigue limit increases from 522 MPa in as machined condition to 636 MPa with shot-peening treatment. SP fatigue limit is even higher than for the mirror polished condition, 615 MPa [42]. The fatigue endurance improvement is the main purpose of the application of this kind of mechanical treatment [73]. Once again, the concept of effective mean stress can be introduced to evaluate the improvement in fatigue life of the shot-peening treatment in comparison with mirror polished and the as machined condition [69]. These effective mean stresses have a value of −84 MPa and −586 MPa respectively.

Failure cross-section observed for SP samples and machined samples at different applied stress levels show that shot-peening surface treatment favours the multiple crack initiation on the surface. With the increase of stress applied level, the number of crack initiation points increases.

The residual compressive stress field introduced by shot-peening,

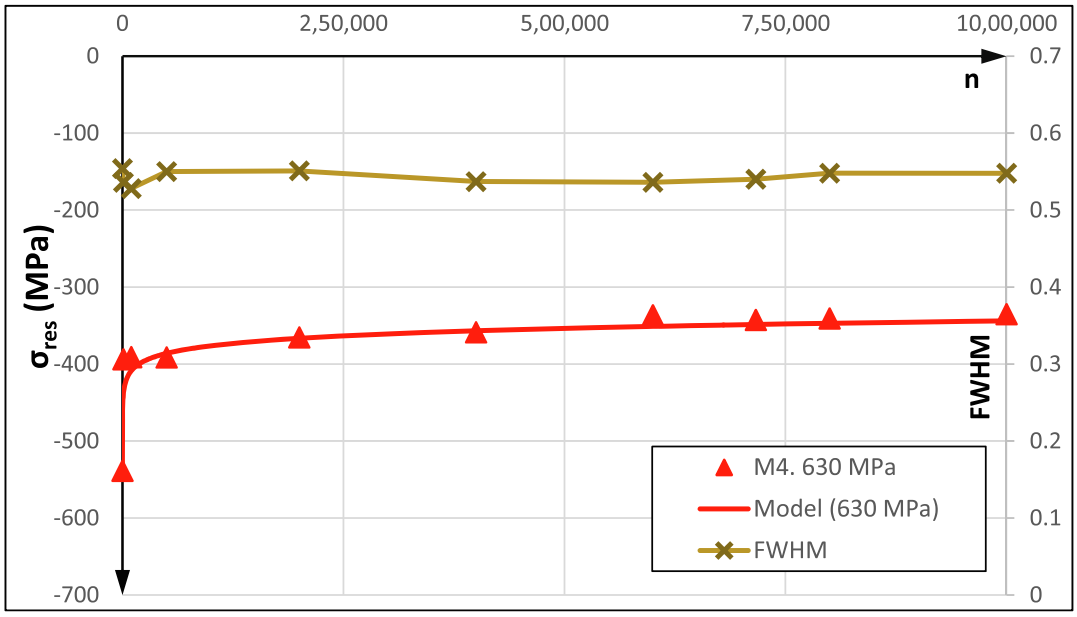

Fig. 19. Surface residual stress relaxation & FWHM for case M3. 703 MPa.

tends to relax/reduce when an external stress is applied. This mechanical residual stress relaxation phenomenon is related to the onset of plastic strains, due to high magnitude stresses which achieves the yield point.

Two types of quasi-static tests were performed, T-C and C-T, with the purpose of identifying the applied stress direction, tensile or compressive. They mainly generate residual stress relaxation. Furthermore, these tests were performed at 6 different applied stress magnitudes, in order to evaluate the influence of stress magnitude on the relaxation. These magnitudes were set close to the monotonic yield point (1084 MPa). In addition, two magnitudes of ± 850 MPa and ± 630 MPa, were set to complete the stress magnitude range applied with cyclic tests.

Principal conclusions obtained from the quasi-static tests, are the following.

- The main relaxation of the residual stress field happens when compressive stress is applied and the effective stress in the external ring of the sample, exceeds the monotonic yield strength.
- Stress relaxation is directly proportional to the applied stress magnitude.

R: −1 axial cyclic tests were performed with four applied stress magnitudes: σ_1: ±849 MPa, σ_2: ±776 MPa, σ_3: ±703 MPa and σ_4: ±630 MPa ($\Delta\sigma$: 73 MPa). The first case, σ_1, with the highest stress magnitude, is placed within LCF and this high applied stress leads to severe plastic strains. The same situation can be found in the second case, σ_2, although, the lower stress applied leads to a slightly lower ratio of plastic strain compared to total strain. In the third case, σ_3, the applied stress is further reduced, so plastic strain generated while cycling, has a smaller role compared to the total strain. For the last stress case, σ_4, its stress magnitude is below the fatigue limit, therefore, the importance and magnitude of plastic strain generated is significantly limited.

Under cyclic loading, this Q + T DIN 34CrNiMo6 steel tends to follow cyclic-softening, which means that the cyclic yield point is lower than monotonic yield point. The cyclic yield point for this material is set in 825 MPa. The consequence of the cyclic-softening tendency of the base material is the increase of residual stress relaxation.

A model to predict the surface residual stress relaxation in terms of the number of applied stress cycles, for different stress magnitude is presented. In this model, the cyclic yield point is considered as the threshold for the onset of plastic strains, from the first cycle. The ratio of produced plastic strains is included by means of coefficient α, which relates the applied stress magnitude with the magnitude of the cyclic yield point. Finally, a logarithmic cycling factor is introduced because relaxation follows a logarithmic reduction, as demonstrated in Fig. 11.

The next principal conclusions that can be extracted from cyclic relaxation tests data are the following.

- The residual stress relaxation increases with the magnitude of the applied stress, due to the increase of generated plastic strains.
- An important stress relaxation occurs in the initial cycles, due to the higher stress magnitude (applied stress plus residual stress) with respect to yield point.
- For the two first cases, σ_1 and σ_2, with the highest stress applied (higher plastic strains generated), the relaxation rate continues until the end of fatigue life.
- The stabilized residual stress level, where residual stress converges, only takes places at low applied stress levels (σ_3 and σ_4).
- The relaxation process under axial fatigue loading has higher relaxation rate than under rotating bending fatigue loading.

The evolution with the number of cycles of the FWHM parameter, in the four applied stress cases, is quite well representative of the situation of the relaxation process [22]. For the first two cases, with higher plastic strains associated, its variation is pronounced and tends to reduce to the base material FWHM value as the residual stress field tends to neutralise. However, in the last two cases, with lower stress applied and lower plastic strain ratio, FWHM remains steady except in the initial cycles, when the relaxation rate shows the greatest magnitude.

Declaration of Competing Interest

The authors declare that they have no known competing financial interests or personal relationships that could have appeared to influence the work reported in this paper.

Acknowledgments

The authors wish to acknowledge the financial support received from the Department of Research and Development of the Basque Government, the UPV/EHU University, through the Research Project Reference: Grupos GV IT947-16.

References

[1] Mitrovic S, Adamovic D, Zivic F, Dzunic D, Pantic M. Friction and wear behavior of shot peened surfaces of 36CrNiMo4 and 36NiCrMo16 alloyed steels under dry and lubricated contact conditions. Appl Surf Sci Jan. 2014;290:223–32. https://doi.org/10.1016/j.apsusc.2013.11.050.

[2] Azar V, Hashemi B, Rezaee Yazdi M. The effect of shot peening on fatigue and corrosion behavior of 316L stainless steel in Ringer's solution. Surf Coat Technol 2010;204(21-22):3546–51.

[3] Niku-Lari A. Shot-peening. International Conferences on Shot Peening. ISCP-1 1981.

[4] Kobayashi M, Matsui T, Murakami Y. Mechanism of creation of compressive residual stress by shot peening. Int J Fatigue 1998;20(5):351–7. https://doi.org/10.1016/S0142-1123(98)00002-4.

[5] Totten GE, Howes MAH, Inoue T. *Handbook of residual stress and deformation of steel*. ASM Int 2002.

[6] Javidi A, Rieger U, Eichlseder W. The effect of machining on the surface integrity and fatigue life. Int J Fatigue Oct. 2008;30(10–11):2050–5. https://doi.org/10.1016/j.ijfatigue.2008.01.005.

[7] Nascimento MP, Souza RC, Pigatin WL, Voorwald HJC. Effects of surface treatments on the fatigue strength of AISI 4340 aeronautical steel. Int J Fatigue 2001;23:607–18. https://doi.org/10.1016/S0142-1123(01)00015-9.

[8] Delosrios E, Walley A, Milan M, Hammersley G. Fatigue crack initiation and propagation on shot-peened surfaces in A316 stainless steel. Int J Fatigue 1995;17(7):493–9. https://doi.org/10.1016/0142-1123(95)00044-T.

[9] Torres MAS, Voorwald HJC. An evaluation of shot peening, residual stress and stress relaxation on the fatigue life of AISI 4340 steel. Int J Fatigue 2002;24:877–86. https://doi.org/10.1016/S0142-1123(01)00205-5.

[10] Bagherifard S, Ghelichi R, Guagliano M. Numerical and experimental analysis of surface roughness generated by shot peening. Appl Surf Sci Jul. 2012;258(18):6831–40. https://doi.org/10.1016/j.apsusc.2012.03.111.

[11] Noyan IC, Cohen JB. Residual stress: measurement by diffraction and interpretation. Springer; 2013.

[12] Vielma AT, Llaneza V, Belzunce FJ. Shot peening intensity optimization to increase the fatigue life of a quenched and tempered structural steel. Proc Eng 2014;74:273–8. https://doi.org/10.1016/j.proeng.2014.06.261.

[13] Prevéy PS, Cammett JT. The Effect of Shot Peening Coverage on Residual Stress, Cold Work and Fatigue in a Ni-Cr-Mo Low Alloy Steel. International Conferences on Shot Peening. ICSP-8 2002.

[14] Laamouri A, Sidhom H, Braham C. Evaluation of residual stress relaxation and its effect on fatigue strength of AISI 316L stainless steel ground surfaces: Experimental and numerical approaches. Int J Fatigue 2013;48:109–21. https://doi.org/10.1016/j.ijfatigue.2012.10.008.

[15] McCLUNG RC. A literature survey on the stability and significance of residual stresses during fatigue. Fatigue Fract Eng Mater Struct 2007;30(3):173–205. https://doi.org/10.1111/j.1460-2695.2007.01102.x.

[16] Vöhringer O. Relaxation of residual stresses by annealing or mechanical treatment. Pergamon Press, Advances Surface Treatments Technology–Applications–Effects 1987;4:367–96.

[17] Fathallah R, Laamouri A, Sidhom H, Braham C. High cycle fatigue behavior prediction of shot-peened parts. Int J Fatigue Oct. 2004;26(10):1053–67. https://doi.org/10.1016/j.ijfatigue.2004.03.007.

[18] Holzapfel H, Schulze V, Vöhringer O, Macherauch E. Residual stress relaxation in an AISI 4140 steel due to quasistatic and cyclic loading at higher temperatures. Mater Sci Eng 1998;248(1-2):9–18. https://doi.org/10.1016/S0921-5093(98)00522-X.

[19] Bignonnet A. Fatigue strenght of shot-peened grade 35NCD 16 steel. Variation of residual stresses introduced by shot peening according to type of loading. International Conferences on Shot Peening. ICSP-3 1987.

[20] Llaneza V, Belzunce FJ. Study of the effects produced by shot peening on the surface of quenched and tempered steels: roughness, residual stresses and work hardening. Appl Surf Sci Nov. 2015;356:475–85. https://doi.org/10.1016/j.apsusc.2015.08.110.

[21] Tosha K, Lu J, Delphine R, Guelorget B, Iida K. Influence of pre-annealing on surface and surface layer characteristics produced by shot peening. International Conferences on Shot Peening. ICSP-8 2002.

[22] Dalaei K, Karlsson B, Svensson LE. Stability of shot peening induced residual stresses and their influence on fatigue lifetime. Mater Sci Eng, A Jan. 2011;528(3):1008–15. https://doi.org/10.1016/j.msea.2010.09.050.

[23] Vaara J, Kunnari A, Frondelius T. Literature review of fatigue assessment methods in residual stressed state. Eng Fail Anal 2020;110:104379. https://doi.org/10.1016/j.engfailanal.2020.104379.

[24] Cammett JT, Sauer CA, Arnold TE. Observations on shot peening residual stresses in 17 Cr-7 Ni austenitic stainless steel and their redistribution via mechanical loading. International Conferences on Shot Peening. ISCP-5 1993.

[25] Benedetti M, Bortolamedi T, Fontanari V, Frendo F. Bending fatigue behaviour of differently shot peened A1 6082 T5 alloy. Int J Fatigue Aug. 2004;26(8):889–97. https://doi.org/10.1016/j.ijfatigue.2003.12.003.

[26] Benedetti M, Fontanari V, Scardi P, Ricardo CLA, Bandini M. Reverse bending fatigue of shot peened 7075–T651 aluminium alloy: The role of residual stress relaxation. Int J Fatigue 2009;31(8–9):1225–36. https://doi.org/10.1016/j.ijfatigue.2008.11.017.

[27] Xie L, Wen Y, Zhan K, Wang L, Jiang C, Ji V. Characterization on surface mechanical properties of Ti–6Al–4V after shot peening. J Alloy Compd 2016;666:65–70. https://doi.org/10.1016/j.jallcom.2016.01.119.

[28] Buchanan DJ, John R. Residual stress redistribution in shot peened samples subject to mechanical loading. Mater Sci Eng, A Oct. 2014;615:70–8. https://doi.org/10.1016/j.msea.2014.06.118.

[29] Zhuang WZ, Halford GR. Investigation of residual stress relaxation under cyclic load. Int J Fatigue 2001;23:31–7. https://doi.org/10.1016/S0142-1123(01)00132-3.

[30] Wick A, Schulze V, Vöhringer O. Effects of warm peening on fatigue life and relaxation behaviour of residual stresses in AISI 4140 steel. Mater Sci Eng 2000;293(1-2):191–7. https://doi.org/10.1016/S0921-5093(00)01035-2.

[31] Harada Y, Mori K. Effect of processing temperature on warm shot peening of spring steel. J Mater Process Technol 2005;162-163:498–503.

[32] Menig R, Schulze V, Löhe D, Vöhringer O. Shot peening plus subsequent short-time annealing-A way to increase the residual stress stability and alternating bending strength of AISI 4140. *SAE Technical Paper*; 2002. p. 711–8, doi: 10.4271/2002/-01-1409.

[33] Bagherifard S, Guagliano M. Fatigue behavior of a low-alloy steel with nanostructured surface obtained by severe shot peening. Eng Fract Mech 2012;81:56–68. https://doi.org/10.1016/j.engfracmech.2011.06.011.

[34] Bagherifard S, Fernandez-Pariente I, Ghelichi R, Guagliano M. Effect of severe shot peening on microstructure and fatigue strength of cast iron. Int J Fatigue 2014;65:64–70. https://doi.org/10.1016/j.ijfatigue.2013.08.022.

[35] Zhang W, Lu J, Luo K. Residual stress distribution and microstructure at a laser spot of AISI 304 stainless steel subjected to different laser shock peening impacts. Metals (Basel) 2016;6(1):Dec. https://doi.org/10.3390/met6010006.

[36] Prevéy PS, Cammett JT. The influence of surface enhancement by low plasticity burnishing on the corrosion fatigue performance of AA7075-T6. Int J Fatigue 2004;26(9):975–82. https://doi.org/10.1016/j.ijfatigue.2004.01.010.

[37] Menig I, Scliulze V, Vöhringer O. Comparison of surface characteristics and thermal residual stress relaxation of laser peened and shot peened AISI 4140. International Conferences on Shot Peening. ICSP-8 2002.

[38] Yang S, Zeng Wu, Yang J. Characterization of shot peening properties and modelling on the fatigue performance of 304 austenitic stainless steel. Int J Fatigue 2020;137:105621. https://doi.org/10.1016/j.ijfatigue.2020.105621.

[39] Kodama S. The behavior of residual stress during fatigue stress cycles. Proceedings of the International Conference on Mechanical Behavior of Metals II 1972;2:111–8.

[40] Avilés R, Albizuri J, Rodríguez A, López De Lacalle LN. Influence of low-plasticity ball burnishing on the high-cycle fatigue strength of medium carbon AISI 1045 steel. Int J Fatigue 2013;55:230–44. https://doi.org/10.1016/j.ijfatigue.2013.06.024.

[41] Avilés A, Avilés R, Albizuri J, Pallarés-Santasmartas L, Rodríguez A. Effect of shot-peening and low-plasticity burnishing on the high-cycle fatigue strength of DIN 34CrNiMo6 alloy steel. Int J Fatigue Feb. 2019;119:338–54. https://doi.org/10.1016/j.ijfatigue.2018.10.014.

[42] Pallarés-Santasmartas L, Albizuri J, Avilés A, Avilés R. Mean Stress Effect on the Axial Fatigue Strength of DIN 34CrNiMo6 Quenched and tempered Steel. Metals (Basel) 2018;8(213). https://doi.org/10.3390/met8040213.

[43] Rodríguez A, López de Lacalle LN, Celaya A, Lamikiz A, Albizuri J. Surface improvement of shafts by the deep ball-burnishing technique. Surf Coat Technol 2012;206(11):2817–24. https://doi.org/10.1016/j.surfcoat.2011.11.045.

[44] UNE-EN ISO. ISO 6892-1:2020 Metallic materials – tensile testing – Part 1: method of test at room temperature (ISO 6892-1:2019).

[45] Boller C, Seeger T. Materials data for cyclic loading: Low-alloy steels, vol. 42. Elsevier; 2013.

[46] Branco R, Costa JD, Antunes FV. Low-cycle fatigue behaviour of 34CrNiMo6 high strength steel. Theor Appl Fract Mech 2012;58(1):28–34.

[47] Branco R, Costa JDM, Antunes FV, Perdigão S. Monotonic and cyclic behavior of DIN 34CrNiMo6 tempered alloy steel. Metals (Basel) 2016;6(5). https://doi.org/10.3390/met6050098.

[48] Smith RW, Hirschberg MH, Manson SS. Fatigue behavior of materials under strain cycling in low and intermediate life range. National Aeronautics and Space Administration Cleveland Oh Lewis Research Center 1963.

[49] ASTM International. ASTM E466–15 Standard practice for conducting force controlled constant amplitude axial fatigue tests of metallic materials. ASTM International 2015. https://doi.org/10.1520/E0466-15.

[50] Fitzpatrick ME, Fry AT, Holdway P, Kandil FA, Shackleton J, Suominen L. Determination of residual stresses by X-ray diffraction; 2005.

[51] SAE International. *Residual stress measurement by X-ray diffraction HS-784/2003*. SAE International; 2003.

[52] Moore MG, Evans WP. Mathematical correction for stress in removed layers in X-ray diffraction residual stress analysis. SAE Trans 1958;66:340–5.

[53] Iida K, Taniguchi K. Relaxation of residual stress distribution produced by shot peening under fatigue test. International Conferences on Shot Peening. ICSP-6 1996.

[54] García-Granada AA, Gomez-Gras G, Jerez-Mesa R, Travieso-Rodriguez JA, Reyes G. Ball-burnishing effect on deep residual stress on AISI 1038 and AA2017-T4. Mater Manuf Processes Aug. 2017;32(11):1279–89. https://doi.org/10.1080/10426914.2017.1317351.

[55] Burgahn F, Vöhringer O, Macherauch E. Microstructural investigations of the shot-peened steel 42 CrMo 4 in different heat treatment conditions by the aid of a X-ray profile analysis. International Conferences on Shot Peening. ICSP-4 1990.

[56] Nazakawa H, Kodama S. Statistical SN testing method with 14 specimens: JSME standard method for determination of SN curve. Statist Res Fatigue Fract-Current Japanese Mater Res 1987;2:55–69.

[57] Davoli P, Bernasconi A, Filippini M, Foletti S, Papadopoulos Iv. Independence of the torsional fatigue limit upon a mean shear stress. Int J Fatigue 2003;25(6):471–80. https://doi.org/10.1016/S0142-1123(02)00174-3.

[58] Ramberg W, Osgood WR. Description of stress-strain curves by three parameters (No. NACA-TN-902). *National Advisory Committee for Aeronautics*, vol. 902; 1943.
[59] Basquin OH. The exponential law of endurance tests. Am Soc Test Mater Proc 1910; 10:625–30.
[60] Hanagarth H, Vöhringer O, Macherauch E. Relaxation of shot peening residual stresses of the steel 42 CrMo 4 by tensile or compressive deformation. International Conferences on Shot Peening. ISCP-4 1990.
[61] Schulze V, Lang KH, Vöhringer O, Macherauch E. Relaxation of shot peening induced residual stresses in quenched and tempered steel AISI 4140 due to uniaxial cyclic deformation. International Conferences on Shot Peening. ISCP-6 1996.
[62] Sakamoto J, Lee Y-S, Cheong S-K. Effect of surface flaw on fatigue strength of shot-peened medium-carbon steel. Eng Fract Mech 2015;133:99–111. https://doi.org/10.1016/j.engfracmech.2014.11.005.
[63] Hua Y, Liu Z, Wang B, Hou X. Surface modification through combination of finish turning with low plasticity burnishing and its effect on fatigue performance for Inconel 718. Surf Coat Technol Oct. 2019;375:508–17. https://doi.org/10.1016/j.surfcoat.2019.07.057.
[64] Marin J. Mechanical behavior of engineering materials. Prentice-Hall; 1962.
[65] Norton J. Machine design: an integrated approach. 3rd ed. New Jersey: Pearson International Edition; 2006.
[66] Avilés R. Métodos de cálculo de fatiga para ingeniería. Madrid: Paraninfo; 2015.
[67] Faupel JH, Fisher FE. Engineering design: A synthesis of stress analysis and materials engineering. New York: Wiley-Interscience; 1981.
[68] Juvinall RC, Saunders H. Fundamentals of machine component design. J Mech Trans Autom Design 1983.
[69] Avilés R, Albizuri J, Lamikiz A, Ukar E, Avilés A. Influence of laser polishing on the high cycle fatigue strength of medium carbon AISI 1045 steel. Int J Fatigue Nov. 2011;33(11):1477–89. https://doi.org/10.1016/j.ijfatigue.2011.06.004.
[70] Holzapfel H, Schulze V, Vöhringer O, Macherauch E. Relaxation behaviour of shot peening induced residual stresses in AISI 4140 due to quasistatic uniaxial loading at elevated temperatures. International Conferences on Shot Peening. ICSP-6 1996.
[71] Kirk D. Effects of plastic straining on residual stresses induced by shot-peening. International Conferences on Shot Peening. ICSP-3 1987.
[72] Wagner L, Luetjering G. Influence of shot peening on the fatigue behavior of titanium alloys. International Conferences on Shot Peening. ICSP-1 1981.
[73] Real E, Rodríguez C, Belzunce FJ, Sanjurjo P, Canteli AF, Fernández-Pariente I. Fatigue behaviour of duplex stainless steel reinforcing bars subjected to shot peening. Fatigue Fract Eng Mater Struct 2009;32(7):567–72. https://doi.org/10.1111/j.1460-2695.2009.01360.x.